[1] Department of Physics and Meteorology, Indian Institute of Technology, Kharagpur, India
[2] Indian National Center for Ocean Information System, Hyderabad, India
[3] Departments of Agronomy and Earth and Atmospheric Sciences, Purdue University, West Lafayette, IN, USA
[4] Office of Biological and Environmental Research, Office of Science, Department of Energy, Germantown, MD, USA

The effect of satellite and conventional meteorological data assimilation on the mesoscale modeling of monsoon depressions over India

V. F. Xavier[1], A. Chandrasekar[1], H. Rahman[2], D. Niyogi[3], K. Alapaty[4]

With 17 Figures

Summary

The Fifth Generation Mesoscale Model (MM5) is used to study the effect of assimilated satellite and conventional data on the prediction of three monsoon depressions over India using analysis nudging. The satellite data comprised the vertical profiles of temperature and humidity (NOAA-TOVS: – National Oceanic and Atmospheric Administration-TIROS Operational Vertical Sounder; MODIS: – MODerate resolution Imaging Spectroradiometer) and the surface wind vector over the sea (QuikSCAT: – Quick Scatterometer); the conventional meteorological data included the upper-air and surface data from the India Meteorological Department (IMD). Two sets of numerical experiments are performed for each case: the first set, NOFDDA (no nudging), utilizes NCEP reanalysis (for the initial conditions and lateral boundary conditions) in the simulation, the second set, FDDA, employs the satellite and conventional meteorological data for an improved analysis through analysis nudging. Two additional experiments are performed to study the effect of increased vertical and horizontal resolution as well as convective parameterization for one of the depressions for which special fields observations were available. The results from the simulation are compared with each other and with the analysis and obser-

vations. The results show that the predicted sea level pressure (SLP), the lower tropospheric cyclonic circulation, and the precipitation of the FDDA simulation reproduced the large-scale structure of the depression as manifested in the NCEP reanalysis. The simulation of SLP using no assimilation high-resolution runs (HRSKF10KM, HRSKF3.3KM) with the Kain-Fritsch cumulus parameterization scheme appeared poor in comparison with the FDDA run, while the no assimilation high-resolution runs (HRSGR10KM, HRSGR3.3KM) with the Grell cumulus scheme provided better results. However, the space correlation and the root mean square (rms) error of SLP for the HRSKF10KM was better than the FDDA; the largest and smallest space correlation for HRSKF10KM, FDDA, and HRSGR10KM were 0.894 and 0.623, 0.663 and 0.195, and 0.733 and 0.338 respectively; the smallest and largest rms error for HRSKF10KM, FDDA and HRSGR10KM were 1.879 and 5.245, 2.308 and 4.242, and 2.055 and 4.909 respectively. The precipitation simulations with the 3.3 km high-resolution, no assimilation runs performed no better than the precipitation simulation with the FDDA run. Thus, a significant finding of this study is that over the Indian monsoon region, the improvements in the simulation using nudging in the FDDA run are of similar magnitude (or better) than the improvements in the simulation due to high-resolution and to cumulus parameterization sensitivity. The improvements in the FDDA run due to analysis nudging were also verified in two more depression cases. The current operational regional models in India do not incorporate the

Correspondence: Anatharaman Chandrasekar, Department of Physics and Meteorology, Indian Institute of Technology, Kharagpur 721302, India (E-mail: chand@phy.iitkgp.ernet.in)

data assimilation of NOAA-TOVS/MODIS and QuikSCAT satellite data, and hence the results of this study are relevant to operational forecasters in India and their ongoing efforts to improve weather forecasting using satellite data sets.

1. Introduction

Monsoon depressions are tropical systems, which form over the North Bay of Bengal region during the summer monsoon season and move in a west-northwest direction bringing copious rainfall across the Indian subcontinent. The number of monsoon depressions which occur over India – their strength and their longevity – are the primary contributors to the sum quantity of Indian summer monsoon rainfall and to the frequency of flooding throughout India's central river basins (Nageswara Rao 2001). Accurate forecasting of the monsoon depression is therefore an important meteorological challenge. A number of recent studies have utilized mesoscale models to study monsoon depressions forecasts over India (Potty et al. 2000; Roy Bhowmik and Prasad 2001; Roy Bhowmik 2003).

An inherent component of improving model forecasts involves the improvement of initial conditions. The ingestion of high-resolution observations into the initial analysis using nudging through four-dimensional data assimilation – FDDA is one way of obtaining an accurate initial condition (Kuo and Guo 1989; Stauffer and Seaman 1990; Nielson-Gammon 2004). Since monsoon depressions typically form over the data-sparse sea regions, this study has endeavored to utilize all possible observations (both conventional upper air, surface, as well as satellite) to obtain an improved analysis.

The nudging technique has the advantage of easy implementation and does not have a large computational demand (Alapaty et al. 2001). The technique does have its share of limitations, the chief one being its inability to directly incorporate variables such as radiances, radar reflectivity, and rainfall into the numerical model that three-dimensional and four-dimensional variational methods (3DVAR, 4DVAR) can utilize. The nudging technique is also limited in that the values chosen for the nudging coefficient must be small enough in order to avoid over-adjustments.

Earlier studies have also utilized FDDA nudging to study monsoon depressions, low pressure systems, and tropical cyclones over India (Rajan et al. 2001; Das et al. 2003; Das Gupta et al. 2003; Singh and Pal 2003; Vaidya et al. 2003; Mukhopadhyay et al. 2004; Sandeep et al. 2006; Xavier et al. 2006). A significant body of literature on the assimilation of satellite sounder data into numerical weather prediction models is now available (Gal-Chen et al. 1986; Doyle and Warner 1988; Lipton and Vonder Harr 1990; Lipton et al. 1995; Ruggiero et al. 1999).

In addition to improved initial conditions through assimilation of observations, the performance of a mesoscale model is also dependent on the horizontal and vertical grid sizes as well as the various parameterization schemes used in the model simulation (Pielke 2002). Recently, Venkata Ratnam and Cox (2006) studied the simulation of the monsoon depressions over India for their sensitivity to different cumulus parameterization schemes such as Kain-Fritsch and Grell using the MM5 model. They found that both of the schemes are able to realistically simulate the large-scale features of monsoon depressions and the resolution of the model has a positive impact on the rainfall simulation. Zhang and Wang (2003) studied the dependence of hurricane intensity and structure on the vertical resolution and time step and found that the simulation with increased vertical resolution produced a deeper storm with lower central pressure and more precipitation.

The chief objective of the current study is to investigate the impact of the improved analysis – obtained by ingestion and assimilation of observations – on the simulation of three monsoon depressions' precipitation over India. The relative impact of nudging versus high-resolution model runs and model physics (cumulus convection parameterization) is also investigated. The three depressions occurred from 25–29 July 1999, 25–28 August 2003, and 5–7 October 2003 over the Bay of Bengal. The July 1999 depression formed during the field phase of the 1999 Bay of Bengal Monsoon Experiment (BOBMEX) campaign.

The background of the three different case studies of monsoon depressions is presented in the following section. Section 2.2 outlines the data and observations used in this study. Section 2.3 provides the model description and the design of numerical experiments. Section 3 provides results and discussion, and Sect. 4 describes the conclusions.

2. Experiment overview

In this section we describe the various case studies of the monsoon depressions to be simulated. The observations and the model configurations are also discussed.

2.1 Case studies

2.1.1 Monsoon depression during BOBMEX (25–29 July 1999)

A low-pressure system formed in the North Bay of Bengal on July 25, 1999 which ultimately intensified into a depression on July 27, 1999. The depression intensified into a deep depression on July 28 just before making landfall. The Indian National Satellite (INSAT) infrared (IR) imagery over the Bay of Bengal on 27 July 1999 03 UTC is shown in Fig. 1a which also shows extensive cloud masses resulting from monsoon depression over the northwest Bay of Bengal and the adjacent region. In a time span of 24 h (i.e. by 28 July 1999 03 UTC), the INSAT IR imagery (not shown) indicated that the cloud mass had organized into a deep depression and that the system had crossed over the east coast of India.
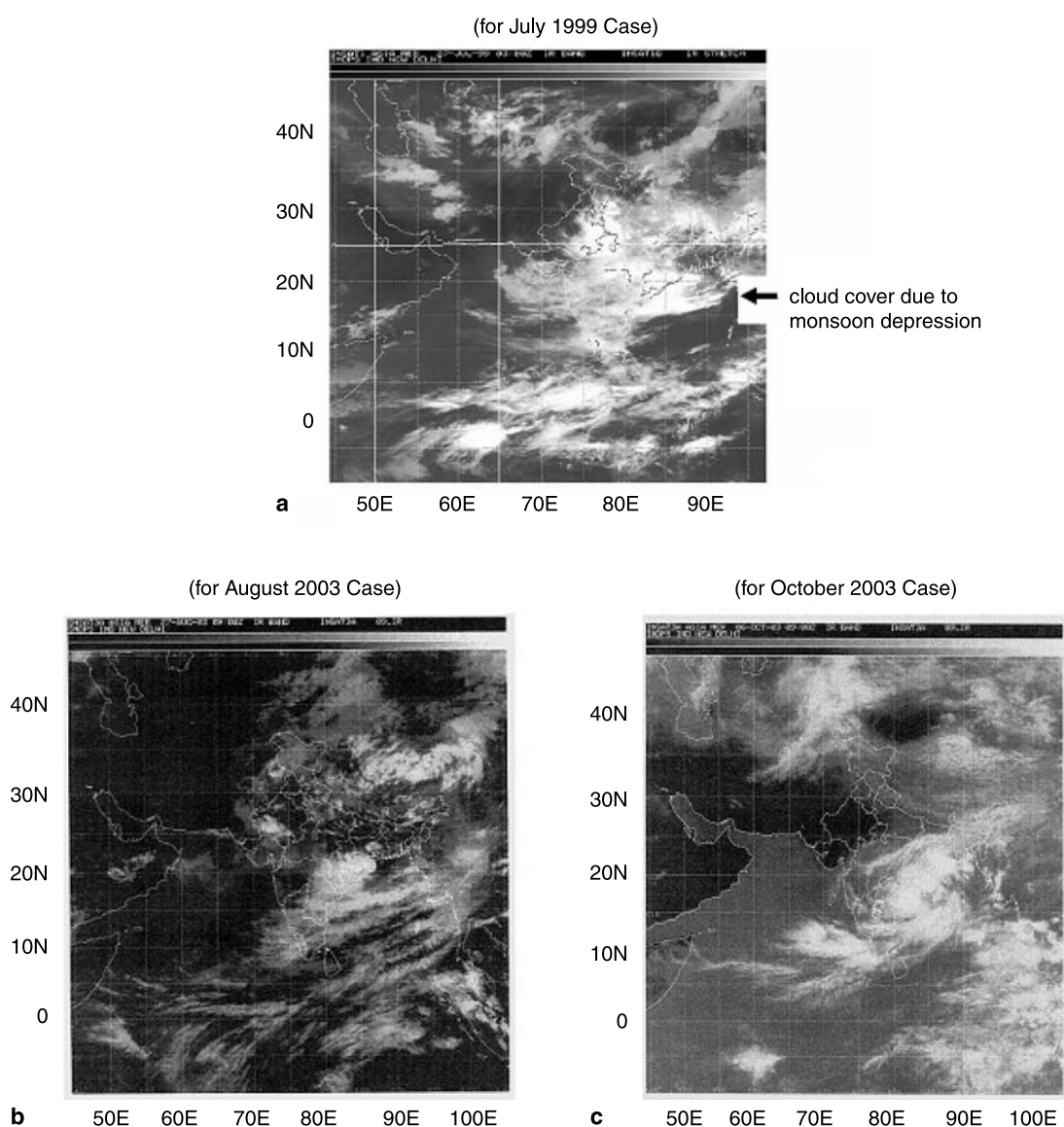
Fig. 1a–c. INSAT IR imagery over India for (**a**) 27 July 1999 03 UTC (**b**) 27 August 2003 09 UTC, and (**c**) 6 October 2003 09 UTC

2.1.2 Monsoon depression from 25–28 August 2003

This monsoon depression first manifested itself as a low-pressure system over the northwest Bay of Bengal off the coast of West Bengal and Orissa on 25 August 2003. The low-pressure system remained stationary at 20.5° N, 88.5° E for the next 48 h and then intensified into a depression in the evening of 27 August 2003. The depression subsequently moved in a west-north-westerly direction and crossed land in the early hours of 28 August 2003. The system moved further westward and weakened into a low-pressure system over the Orissa region on 29 August 2003. In Fig. 1b the INSAT IR imagery on 27

August 2003 at 09 UTC shows extensive cloud cover associated with the monsoon depression over the northwest Bay of Bengal.

2.1.3 Monsoon depression from 4–7 October 2003

This monsoon depression first initiated as a low-pressure system over the south Bay of Bengal and adjoining areas on 4 October 2003. The low-pressure system remained stationary for the next 24 h and was classified as a depression on 6 October 2003. The depression subsequently moved in a northerly direction and crossed the north coast of Andhra Pradesh in the early hours of 7 October 2003 and lay centered at 19° N,
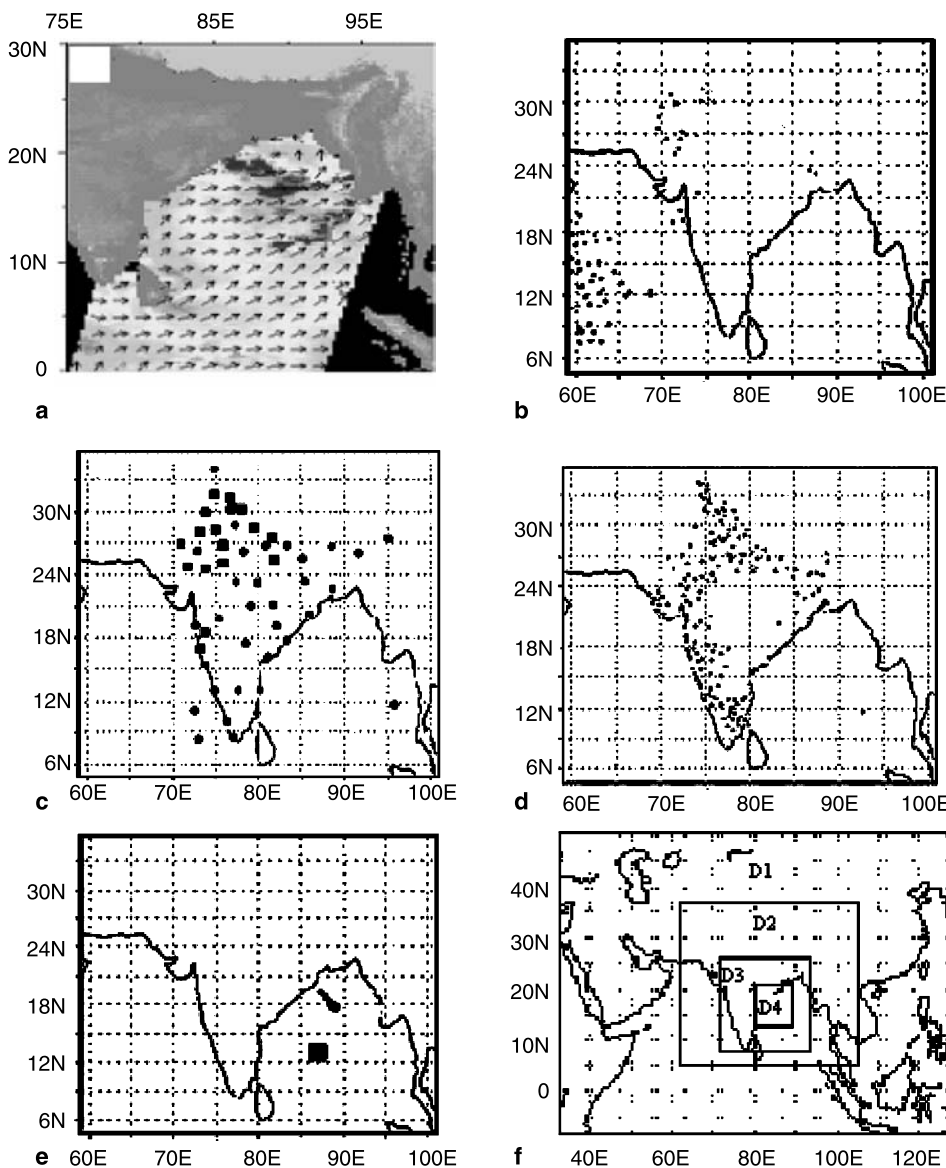
Fig. 2a–f. Typical pass of (**a**) QuikSCAT, (**b**) NOAA-TOVS, (**c**) locations of all IMD upper air stations (filled circles RS/RW and filled squares PB), and (**d**) surface stations. Filled square in (**e**) depicts the BOBMEX buoy location and the line indicates the BOBMEX ship movement towards south-east, and (**f**) shows the MM5 model domains (D1, D2, D3, and D4 are 90, 30, 10, and 3.3 km horizontal resolution)

83° E at 03 UTC on 7 October 2003. The system then moved in an east northeasterly direction and weakened into a low-pressure system over Jharkhand on 9 October 2003. The INSAT IR imagery on 6 October 2003 at 09 UTC (Fig. 1c) showed extensive cloud cover associated with the monsoon depression over the southwest Bay of Bengal.

2.2 Data/observations

The humidity profiles from 6 levels and temperature profiles from 17 levels were utilized from the Television and Infrared Observation Satellite (TIROS) and Operational Vertical Sounder (TOVS) onboard the NOAA satellite (Rajan et al. 2002). Temperature and humidity profiles were used from 14 different vertical levels from MODIS, as well as the surface wind vector over the sea from QuikSCAT. In addition to the satellite observations, the assimilation employed conventional surface observations and IMD upper air: radiosonde/rawinsonde (RS/RW) and pilot balloon (PB) observations. For the July 1999 monsoon depression, special observations (research ships, buoys, INSAT, coastal radar, and other conventional observation systems) over the Bay of Bengal were available from the BOBMEX field program (Sikka and Sanjeeva Rao 2000) and these were used to validate the model performance. Figure 2a–d show how the observations (satellite, conventional upper-air, and surface) were assimilated into the model by using analysis nudging for the BOBMEX depression case. Figure 2e shows the BOBMEX based buoy and ship location as it moved away from the coast.

2.3 Model description and experiments

The MM5 model version 3.5/3.6 (Grell et al. 1994) with twenty-three vertical layers and two one-way nested domains was utilized. The Outer Domain consisted of 90 km grid spacing with 85×75 grid cells in the east-west (EW) and north-south (NS) directions; the Inner Domain consisted of 30 km grid spacing with 129×119 grid cells in the EW and NS directions.

Two numerical experiments (FDDA and NOFDDA) were designed to study the impact of the satellite data and conventional IMD ob-

servations on the simulated structure of the monsoon depressions. Two additional simulation experiments (HRSGR and HRSKF) were performed for the BOBMEX depression case. The first of these additional experiments examined the effect of increased vertical and horizontal resolutions without assimilation on the prediction of the monsoon depression. The second additional experiment looked at the effect of the Kain-Fritsch convective parameterization scheme over the Grell scheme for the increased vertical and horizontal resolutions without assimilation. For these additional increased resolution experiments, in addition to the above 90 and 30 km domains, the model was configured with 35 vertical sigma layers and two additional one-way nested domains having a 10 km horizontal grid spacing with 228×216 grid cells and a 3.3 km grid spacing with 297×288 grid cells in the EW and NS directions.

The other model settings for the BOBMEX depression case included the MRF PBL, the Grell cumulus scheme, Dudhia's simple ice scheme, a simple radiation scheme, and a multi-level soil model. The NCEP reanalysis data available at a horizontal resolution of $2.5° \times 2.5°$ and a time resolution of 6 h were used to develop the initial and lateral boundary conditions for all three depression cases. The model settings for the monsoon depressions in August and October 2003 were the same as the above, except that a mixed phase Reisner scheme was used instead of the simple ice scheme.

The model simulations for the BOBMEX monsoon depression case were performed from 25 July 1999 00 UTC to 29 July 1999 00 UTC and the first numerical experiment (NOFDDA) utilized the NCEP reanalysis for the initial and lateral boundary. Using analysis nudging to improve the NCEP reanalysis, the second numerical experiment (FDDA) for the BOBMEX depression incorporated the NOAA-TOVS, QuikSCAT and IMD soundings as well as surface data gathered over India between 25 July 1999 00 UTC and 26 July 1999 00 UTC. The nudging coefficients used were the default values: $2.5 \times 10^{-4} \, s^{-1}$ for temperature and wind, and $1 \times 10^{-5} \, s^{-1}$ for the mixing ratio. The model was integrated from 26 July 1999 00 UTC to 29 July 1999 00 UTC.

The high-resolution (two additional domains of 10 km and 3.3 km grid size, together with

35 vertical levels) HRSGR (HRSGR10KM and HRSGR3.3KM) experiments used Grell as a cumulus parameterization, while the HRSKF (HRSKF10KM and HRSKF3.3KM) was identical to the HRSGR except that the former utilized Kain Fritsch as the cumulus parameterization scheme. For the 3.3 km domain, the convective parameterization was deactivated during the simulation.

For the August 2003 depression, (NOFDDA), the model simulations were performed from 25 August 2003 00 UTC to 28 August 2003 12 UTC using the NCEP reanalysis. To improve the NCEP reanalysis using analysis nudging between 25 August 2003 00 UTC and 26 August 2003 00 UTC the FDDA run for this case incorporated MODIS temperature and humidity profiles, QuikSCAT surface wind vectors and IMD soundings as well as surface data. The model was integrated without nudging from 26 August 2003 00 UTC to 28 August 2003 12 UTC.

For the October 2003 depression (NOFDDA), the model simulations were performed from 4 October 2003 00 UTC to 7 October 2003 12 UTC using the NCEP reanalysis. Data similar to the August case were incorporated into the NCEP reanalysis using analysis nudging between 4 October 2003 00 UTC and 5 October 2003 00 UTC. The model was integrated without nudging from 5 October 2003 00 UTC to 7 October 2003 12 UTC. The August and October 2003 depression cases used nudging coefficients of $1 \times 10^{-4}\,s^{-1}$ for temperature and wind and $1 \times 10^{-6}\,s^{-1}$ for the mixing ratio. The results of the MM5 simulations for all three depressions were then compared with the observations and the NCEP reanalysis. The comparison of the model results for all three depressions was done for the model run in the free-forecast mode.

3. Results and discussions

In this section, first the two experimental runs for the July 1999 depression will be compared. The results for the July 1999 depression were then compared with the BOBMEX special observations and the NCEP reanalysis. In addition, the FDDA results were compared with high-resolution/no assimilation runs using the Grell and Kain Fritsch cumulus parameterization schemes. Subsequently, the two experimental runs for the

August and October 2003 depressions will be compared.

As is commonly known, even with an accurate and optimal data assimilation scheme, marked improvements for every single forecast are not possible. What can be expected, however, is that the forecast error, on average, will be reduced with each assimilation. Consequently, these assimilation experiments need to be extended to similar and independent studies in order to draw broad conclusions on the effects of data assimilation that incorporate nudging. For this reason, this study investigated three similar and independent monsoon depressions over the Bay of Bengal.

3.1 July 1999 monsoon depression

3.1.1 Model evaluations of the NOFDDA and FDDA simulations

The primary objective of this work was to study the effects of satellite and conventional data assimilation using analysis nudging on the simulated structure of monsoon depressions over India. Considering the application of this research to operational forecasting, the ingestion and assimilation of data using analysis nudging was restricted to the first 24 h of model integration, after which the model simulation was in the free-forecast mode. The model domains (90, 30, 10 and 3.3 km horizontal grid sizes) are shown in Fig. 2f. All of the model results discussed here correspond to the 30 km domain except for the two additional high-resolution experiment results, which correspond to 10 and 3.3 km.

Figure 3a–l show the sea-level pressure pattern (SLP) for 26–29 July 1999 for 00 UTC. The figures show the NCEP reanalysis, the NOFDDA, and the FDDA simulations. As is the norm for the Indian monsoon region, because of the lack of high-resolution observations, the reanalysis results were used to verify the model results. A clear improvement was noticeable in the horizontal structure of the SLP field obtained from the ingestion and assimilation of satellite (NOAA-TOVS and QuikSCAT) and conventional meteorological (RS/RW, PB and surface) data using analysis nudging. The monsoon depression's central SLP in the NOFDDA simulation was higher by 4 hPa as compared to the NCEP
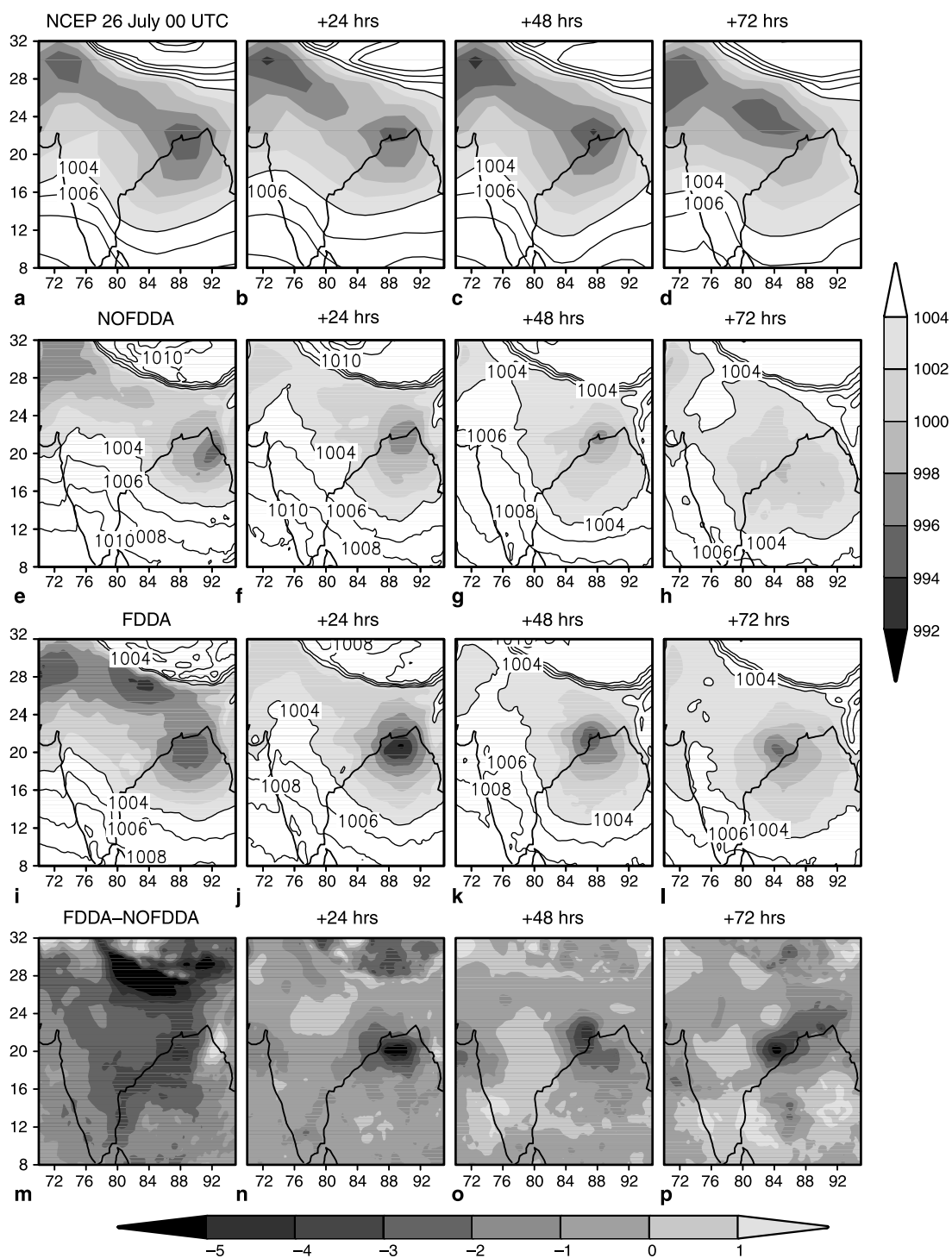
Fig. 3a–l. Sea-level pressure (hPa) for 26 July 1999 00 UTC and for 24, 48, and 72 h of forecast of NCEP reanalysis, NOFDDA and FDDA. (**m–p**) Sea-level pressure difference (hPa) of NOFDDA from FDDA for the 26 July 1999 00 UTC and for 24, 48, and 72 h of forecast

reanalysis and the FDDA simulations. Although some conventional meteorological upper air RS/RW along the east coast of India and the island station Port Blair (11.66° N, 92.71° E)

did contribute to the MM5 model ingestion and assimilation; the results of this study suggest that the improvement seen in the FDDA SLP field for 26 July 1999 00 UTC was mainly due to the

assimilation of NOAA-TOVS temperature and humidity vertical profiles. These assimilations improved the representation of the atmospheric thermodynamic structure. Also, Fig. 3e–h shows that the depression simulated from the NOFDDA run is weak. The MM5 simulation with improved
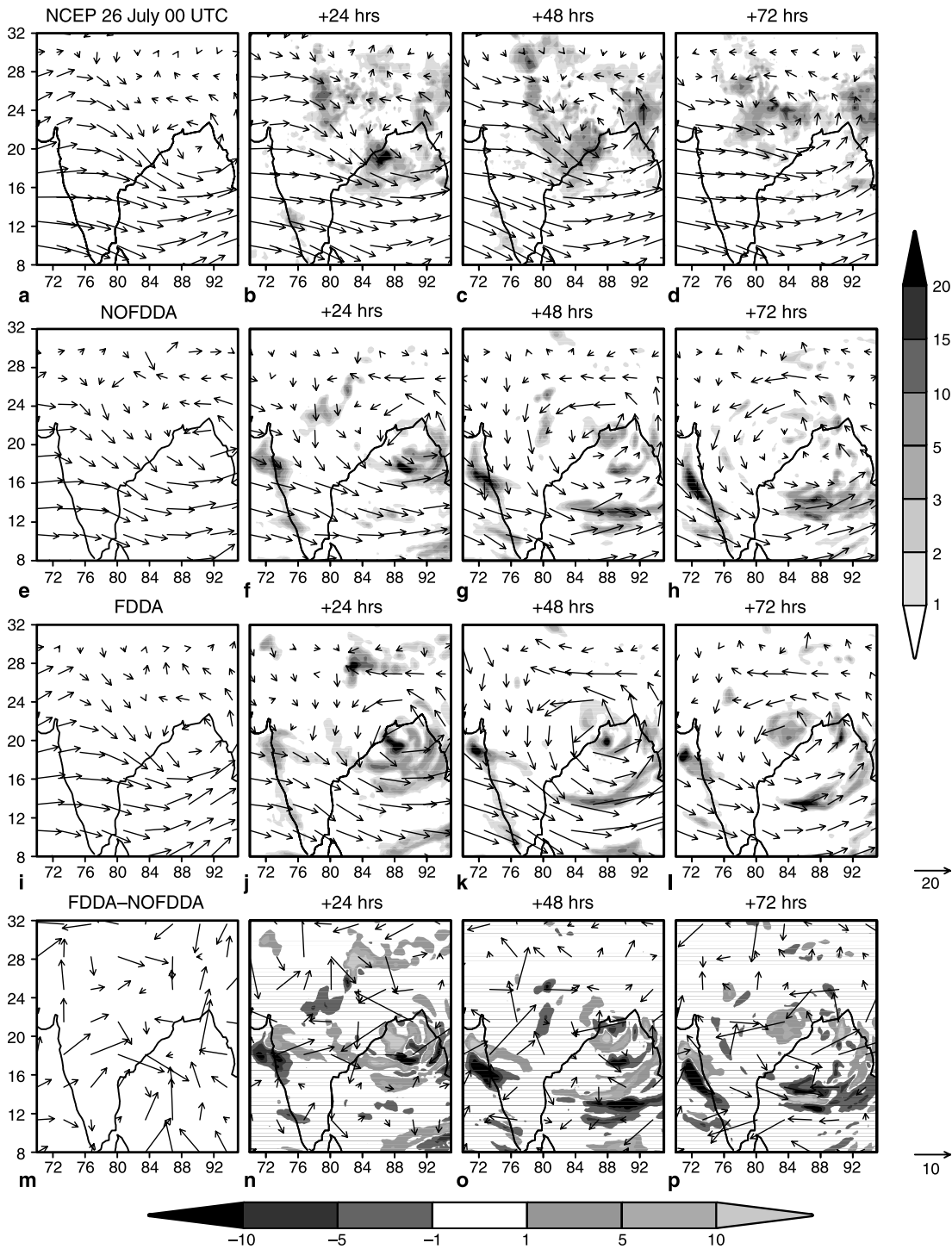
Fig. 4a–l. Lower tropospheric winds (m s^{-1}) (850 hPa for NCEP reanalysis and $\sigma = 0.825$ for MM5 simulations) for 26 July 1999 with 00 UTC and for 24, 48, and 72 h of forecast. Also shown are the 24 h accumulated TRMM rainfall (cm) and the model precipitation (cm) at 24, 48, and 72 h of forecast. (**m–p**) Lower tropospheric wind difference (m s^{-1}) of NOFDDA from FDDA for 26 July 1999 00 UTC and for 24, 48, and 72 h of forecast. Also shown are the 24-hour accumulated precipitation differences (cm) of NOFDDA from FDDA at 24, 48, and 72 h of forecast

analysis (FDDA, Fig. 3i–l), however, indicated a system that approximated much more closely the NCEP reanalysis as compared to the simulation without improved analysis (NOFDDA).

The NCEP reanalysis showed active monsoon conditions characterized by a strong north-south pressure gradient together with the presence of a monsoon depression over the North Bay of Bengal. The results of the NOFDDA and FDDA runs simulated the strong meridional pressure gradient at the beginning of the forecast (Fig. 3e, i). However, only the FDDA run (Fig. 3j–l) simulated the strong monsoon depression as seen in the NCEP reanalysis. Observations indicated that the monsoon depression crossed land on 28 July 1999 and the MM5 simulations reproduced this. Although their horizontal resolution was not very high (about 1 degree latitude longitude), this resolution was finer than the average distance of radiosonde stations (typically about 300 km). The QuikSCAT data had a much higher typical resolution (25 km × 25 km) as compared to the analysis and NOAA-TOVS. Due to the above assimilation of satellite datasets, the FDDA simulation could lead to a better adjustment to the high-resolution observations through the traditional analysis-nudging procedure. The differences between the SLP fields of the FDDA and NOFDDA run on 26 July 1999 00 UTC, and at 24, 48 and 72 h of forecast are shown in Fig. 3m–p. The negative pattern of mean SLP difference of 4 hPa can be seen in the vicinity of the depression center (Fig. 3m–p) indicating that a stronger depression was simulated in the FDDA run.

Figure 4a–l depict the lower tropospheric winds ($\sigma = 0.825$ for MM5 simulations and 850 hPa for NCEP reanalysis) for 26–29 July 1999 for 00 UTC and the 24-hour accumulated precipitation valid for 27–29 July 1999 00 UTC. The assimilation of high-resolution QuikSCAT wind observations in the FDDA run produced a well-developed cyclonic circulation. Figure 4b–d show 24-hour accumulated rainfall from the Tropical Rainfall Measurement Mission (TRMM) valid for 27–29 July 1999 00 UTC. The maximum 24-hour accumulated precipitation from TRMM was seen over the east coast of India as well as the adjacent Bay of Bengal regions on 27 July 1999 00 UTC. The rainfall pattern moved inland for the next two days, consistent with the fact that the depression crossed

land on 28 July 1999. The TRMM 24-hour accumulated rainfall also showed some rainfall over the orographic regions of the west coast of southern India for 27 and 28 July 1999 00 UTC. However, the IMD observed rainfall (not shown here for brevity) did show fairly extensive rainfall along the west coast of India. Neither of the 24-hour accumulated precipitation in both MM5 simulations, FDDA and NOFDDA, revealed marked inland penetration of the rainfall pattern on 28 and 29 July 1999 00 UTC as shown by the TRMM data. The 24-hour accumulated precipitation from the FDDA simulation showed an improved large-scale structure of the spatial precipitation pattern on 27 July 1999 00 UTC. It also showed more rainfall over the eastern coastal areas with more inland penetration of rainfall on 29 July 1999 00 UTC as compared to the NOFDDA simulation. The above result is consistent with Das et al. (2003) who obtained increased amounts of rainfall in the nudging experiments.

The high rainfall amounts attributed to the orographic influence over the Western Ghats in the TRMM observations for 27 and 28 July 1999 00 UTC was well-captured in both the MM5 simulations. This increased accuracy was due to the finer horizontal resolution (30 km) of the MM5 model as compared with the analysis. The simulated rainfall amounts of both the runs over the depression were however lower than the TRMM rainfall data. Although the use of nudging could have contributed to a change in the PBL moisture flux and convergence fields and led to a better rainfall prediction, an assumption that accurate initial conditions alone determine the rainfall forecast in a mesoscale model would be very simplistic. Although Das et al. (2003) found increased amounts of rainfall due to nudging, they also experienced difficulties in the correct simulation of the rainfall maximum location. Figure 4m–p present a) the differences in lower tropospheric wind for 26 July 1999 00 UTC and for 24, 48, and 72 h of forecast and b) the differences in 24 h accumulated rainfall for 24, 48 and 72 h of NOFDDA forecast using the FDDA runs. Figure 4m shows a distinct enhancement of the onshore winds crossing the west coast of India and an enhanced cyclonic circulation in the vicinity of the depression. The above features were also seen at other times, although the cyclonic

circulation is less marked in Fig. 4n–p. The positive value of the 24-hour difference in accumulated rainfall around the depression, especially over the land regions in Fig. 4n–p, lends credence to the earlier FDDA simulation results, which showed increased rainfall over the eastern coastal regions.

3.1.2 Effect of grid spacing and cumulus parameterization schemes

The improved performance of the simulation of any meteorological system can be due to a variety of factors, such as improved data assimilation, higher resolution in both the horizontal and ver-
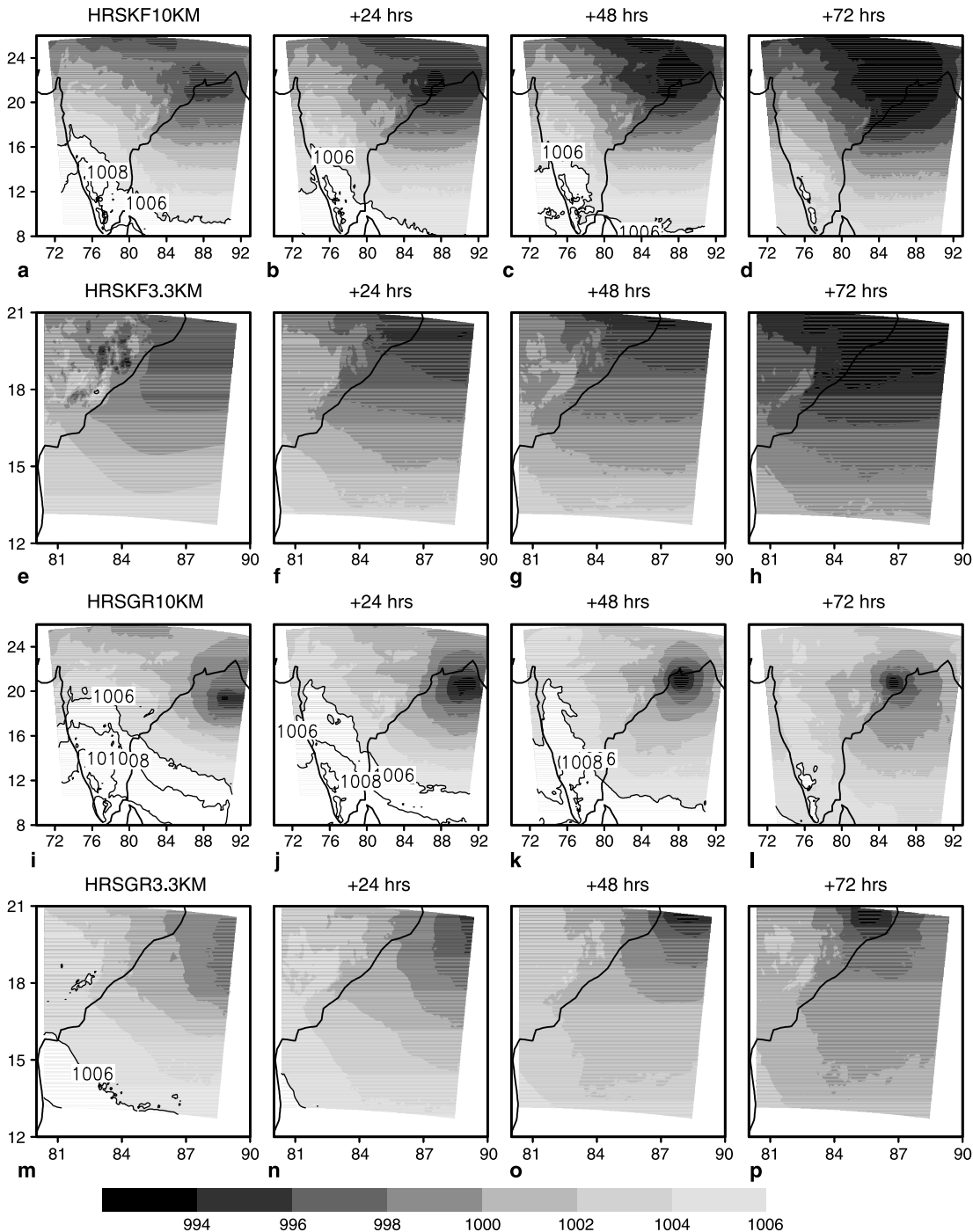
Fig. 5a–p. Sea-level pressure (hPa) for 26 July 1999 00 UTC and for 24, 48, and 72 h of forecast of HRSKF10KM, HRSKF3.3KM, HRSGR10KM and HRSGR3.3KM

tical directions, and/or the use of a better physical parameterization scheme in the model. One can argue that improvements in the simulation due to nudging can be obtained with a higher resolution model in both the horizontal and vertical directions, and with the appropriate choice of cumulus parameterization scheme. Through further analysis nudging tests, two additional experiments demonstrated the importance of data assimilation through nudging: (1) the use
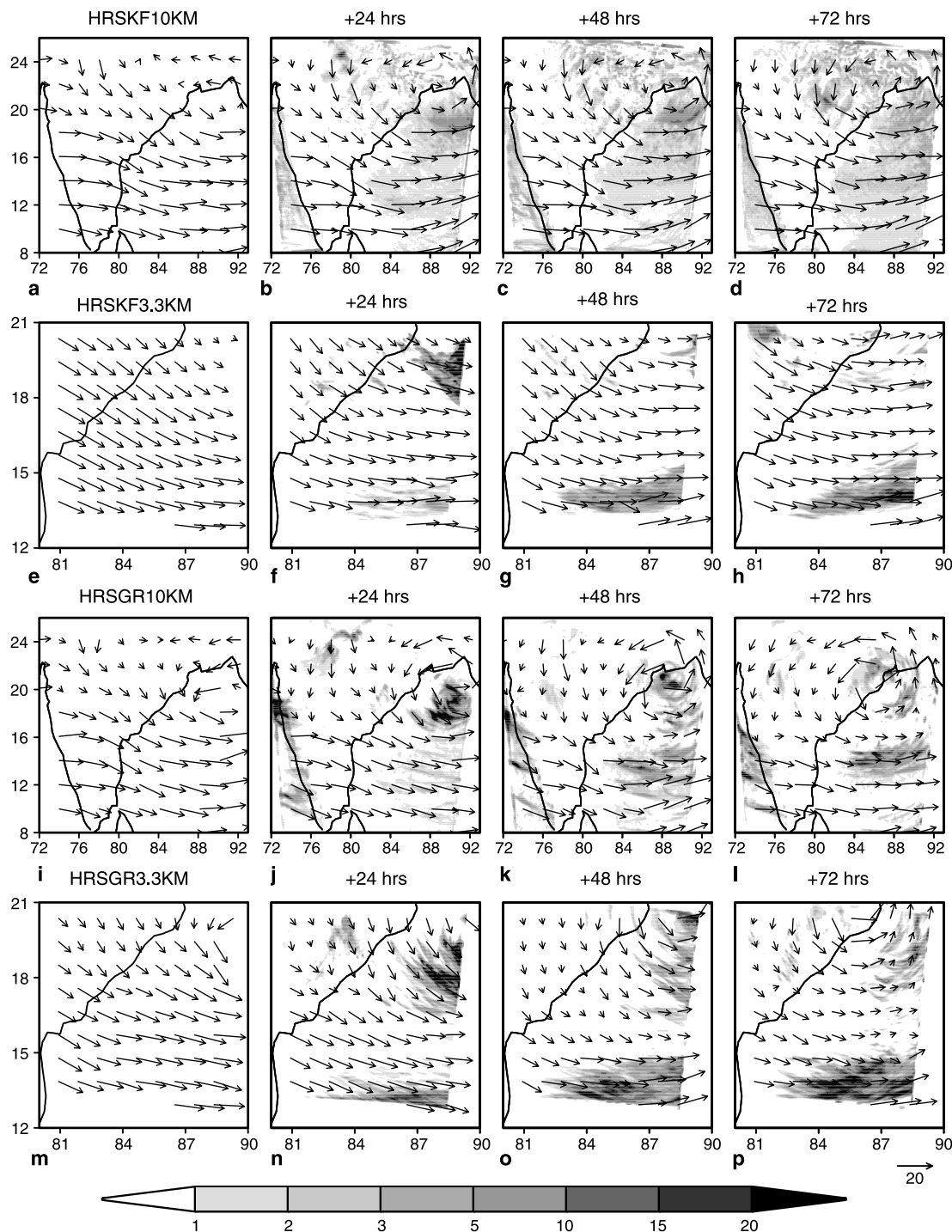
Fig. 6a–p. Lower tropospheric winds (m s^{-1}) ($\sigma = 0.8325$) for 26 July 1999 with 00 UTC and for 24, 48, and 72 h of forecast of HRSKF10KM, HRSKF3.3KM, HRSGR10KM, HRSGR3.3KM. Also shown are the 24 h accumulated model precipitations (cm) at 24, 48, and 72 h of forecast of HRSKF10KM, HRSKF3.3KM, HRSGR10KM, and HRSGR3.3KM

of higher resolution and (2) a better cumulus parameterization scheme. Figure 5a–h shows the SLP pattern for 26–29 July 1999 for 00 UTC from the HRSKF10KM (Fig. 5a–d) and the HRSKF3.3KM (Fig. 5e–h) runs. Figure 5i–p resemble Fig. 5a–h, except that 5i–p refer to the HRSGR10KM and HRSGR3.3KM runs.

The model results in Fig. 5i–p clearly show that both the 10 and 3.3 km correctly simulated the occurrence of the monsoon depression's landfall. However, Fig. 5i–p indicate that the depression did not weaken after crossing landfall as the central lower pressure is about 992 hPa in the high-resolution run. This behavior contrasts with that of the FDDA run which, due to frictional effects, shows a slight weakening of the system after it crossed land. The results of the HRSKF (Fig. 5a–h) run simulate a SLP pattern with the regions of low pressure smeared over a large horizontal region as compared to the Grell (HRSGR) run. The HRSKF run also indicates that the depression had crossed land before the 48-hour mark and this does not agree with the observations.

Figure 6a–h depict the lower tropospheric winds ($\sigma = 0.8325$) for 26–29 July 1999 for 00 UTC and the 24-hour accumulated precipitation valid for 27–29 July 1999 00 UTC for the HRSKF10KM (Fig. 6a–d) and the HRSKF3.3KM (Fig. 6e–h) runs. Figure 6i–p are similar to Fig. 6a–h except that the former refers to the HRSGR10KM and the HRSGR3.3KM runs. Despite an increase in the number of vertical levels and finer grid size, the cyclonic circulation simulated by the HRSGR10KM run (Fig. 6i) is not as well developed as Figure 4i simulated by the FDDA run. Also, the FDDA run-simulated winds are stronger in magnitude (Fig. 4j–l) as compared to the winds in the HRSGR10KM run (Fig. 6j–l). On the other hand, the HRSKF10KM run (Fig. 6a–d) simulates a well-developed and more powerful cyclonic circulation compared to the HRSGR10KM run. The simulated winds are stronger with finer resolution as compared to the 10 km grid size results for both cumulus parameterization schemes.

It was expected that an increase in the vertical and horizontal resolutions would have a positive effect on the performance of the simulated precipitation associated with the depression. A comparison of Fig. 6j–l for the HRSGR10KM run

with Fig. 4j–l for the FDDA run shows that increased levels (to 35) and a finer grid size (to 10 km) did not improve the simulation of depression-associated precipitation. In fact, unlike the FDDA run (Fig. 4j), the HRSGR10KM run (Fig. 6j) shows very little rain over the coastal land regions. The results of the high-resolution HRSKF10KM run (Fig. 6b), despite showing extensive rainfall over the coastal land regions, with hardly any rain above 100 mm, fails to simulate the correct magnitude of rainfall. However, the HRSGR10KM run did simulate precipitation over the Western Ghats region, while the HRSKF10KM simulated only light rain along the west coast. Relatively poor in their accuracy, the simulation of the model rainfall from the HRSGR3.3KM (Fig. 6n–p) and the HRSKF3.3KM (Fig. 6f–h) runs show hardly any rainfall was received over the coastal land regions. In terms of precipitation simulation, both the HRSGR and HRSKF runs without any assimilation have fared poorly compared to the FDDA run, despite an improvement of one order of magnitude in the finer grid size and an increase in the number of vertical levels.

The above result does not undermine the importance of higher resolution, but only highlights the positive impact of meteorological data assimilation and improved initial conditions on the monsoon depression simulation. In a recent study, Mass et al. (2002) report MM5 modeling results, without any assimilation, which suggests that the results of the coarser grid (12 km) verified better with observations than the high-resolution grid (4 km). The MM5 model precipitation skill did not improve with the finer grid spacing from 36 km to 12 km. However, the verification skills of precipitation declined slightly as the resolution decreased from 12 to 4 km. Mass et al. (2002) argue that while the high-resolution results appear to simulate realistic structures, they do not necessarily verify better with observations. This discrepancy is attributed to the fact that the timing and position errors are more heavily penalized with the increase in resolution. Data scarcity, the problem of data accuracy, deficiencies in the physical parameterization of the planetary boundary layer, and the smaller scale surface and moisture budget parameterizations are additional factors leading to the discrepancy. Therefore, the traditional verification

scores such as mean error and mean absolute error can show larger errors for the high-resolution results.

One important point to keep in mind is that due to computational limitations, the 3.3 km model domain did not encompass the entire mon-
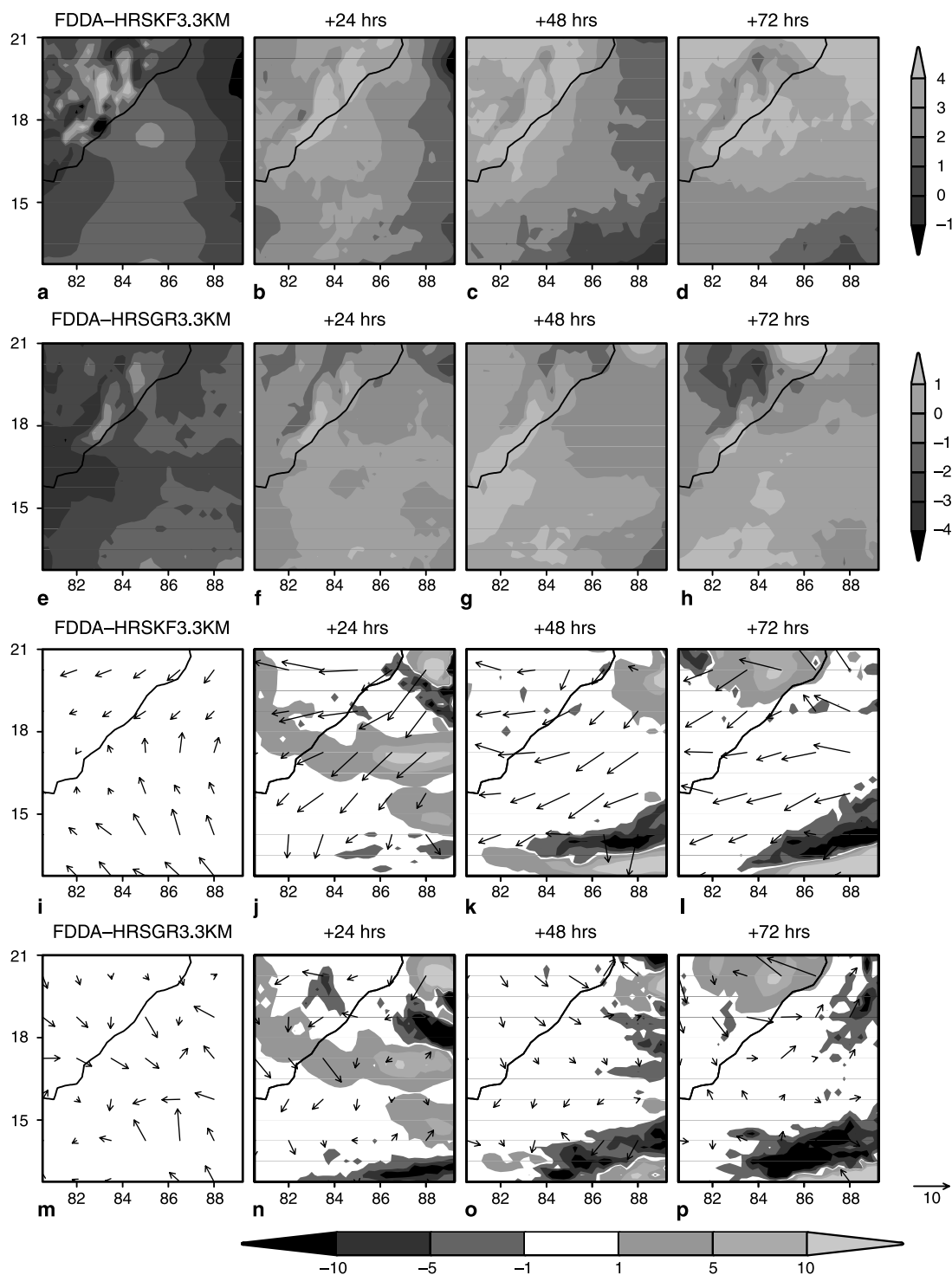
Fig. 7a–d. Sea-level pressure difference (hPa) of HRSKF3.3KM from FDDA for the 26 July 1999 00 UTC and for 24, 48, and 72 h of forecast. (**e–h**) Same as (**a–d**) except for difference of HRSGR3.3KM from FDDA. (**i–l**) Lower tropospheric wind difference (m s^{-1}) of KF3.3KM from FDDA for 26 July 1999 00 UTC and for 24, 48, and 72 h of forecast. Also shown the 24 h accumulated precipitation difference (cm) of KF3.3KM from FDDA at 24, 48, and 72 h of forecast. (**m–p**) Same as (**i–l**) except for the difference of HRSGR3.3KM from FDDA

soon depression. Since the precipitation simulation of the 10 km runs (HRSGR and HRSKF) indicated more precipitation south of the depression, the model domain for the finest grid was chosen such that a larger area south of the depression was present in the innermost domain.

Figure 7a–d depict the difference of the mean SLP field of HRSKF3.3KM from the FDDA run valid at 26 July 1999 00 UTC, and at 24, 48, and 72 h of forecast. Figure 7e–h show the corresponding results for the HRSGR3.3KM run. Both these figures were obtained after regridding the MM5 outputs of 3.3 km and the 30 km FDDA runs to a common horizontal resolution of

$0.25° \times 0.25°$. As can be seen in Fig. 7a and b, up to 24 h of the forecast period, the FDDA run simulated a stronger depression (negative SLP differences) than the HRSKF3.3KM run in the immediate vicinity of the depression center. However the differences changed sign at 48 and 72 h, indicating that the FDDA's effect decreased with increasing forecast duration. Similar results are observed in the HRSGR3.3KM run in Fig. 7e–h. The FDDA run simulated a stronger depression in the vicinity of the depression. After 24 h, the differences of SLP field become positive. The difference in the winds between FDDA and the HRSGR3.3KM run seen in Fig. 7m–p
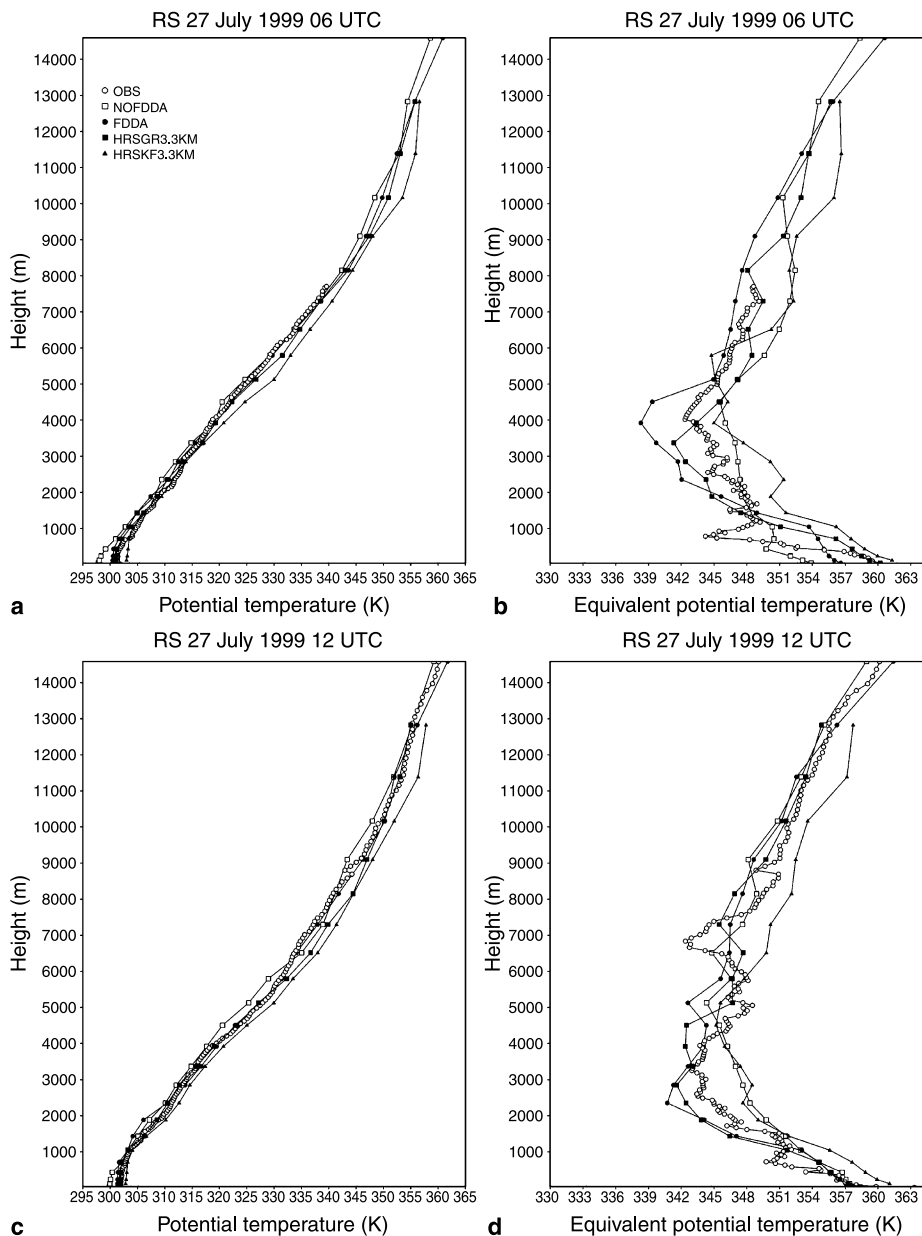
Fig. 8a–d. Comparison of potential temperature – θ (**a** and **c**) and equivalent potential temperature – θ_e (**b** and **d**) in K of BOBMEX and model results for 27 July 1999 06 and 12 UTC

shows a prominent cyclonic circulation at 72 h of forecast (Fig. 7p). A less marked cyclonic circulation at 26 July 1999 00 UTC and at 24, 48 h of forecast is shown in the vicinity of the depression; this indicates that the cyclonic circulation of the FDDA run was stronger than the high resolution Grell run at these times. However, the differences in the wind fields between the FDDA and the HRSKF3.3KM run (Fig. 7i–l) do not show a similar feature, which indicates a stronger cyclonic circulation corresponding to the Kain Fritsch run.

The difference in the precipitation fields between the FDDA run and the high resolution runs (Fig. 7j–l and n–p) were more positive over land

and as the figures show, especially clear at the 72 h forecast where the difference in the precipitation fields for the two cases are about 15 cm or higher. This variation indicates that the FDDA run simulated more rain over the eastern coastal regions with a larger inward penetration of rainfall as compared to the high-resolution runs.

3.1.3 Further model evaluations with BOBMEX special observations

Figure 8a–d depict the potential temperature (θ) and the equivalent potential temperature (θ_e) for 27 July 1999 06 and 12 UTC for the MM5
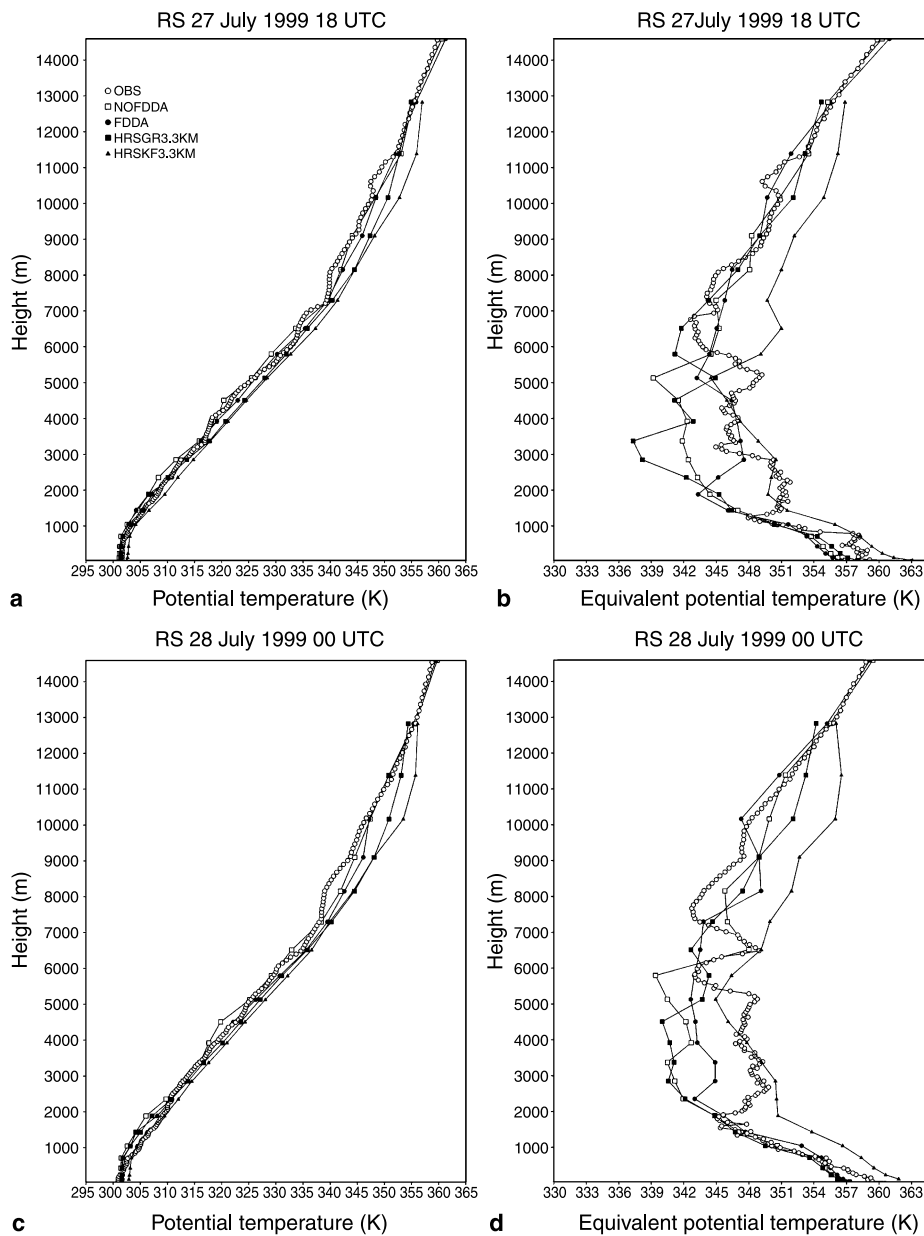
Fig. 9a–d. Same as Fig. 8a–d, except for 27 July 1999 18 UTC, and 28 July 1999 00 UTC

runs and the BOBMEX (17.5° N, 89° E) observations. The θ and θ_e vertical profiles are obtained from the location of the grid cell in the MM5 domains closest to the radiosonde locations. The four model θ profiles compare reasonably well with the BOBMEX observations. Figure 8 shows that the θ_e simulated by the FDDA run and the HRSGR3.3KM run compares more favorably with the BOBMEX observations. However, the HRSKF3.3KM run appears to have overestimated both the θ and the θ_e observed values for 27 July 1999 06 and 12 UTC (Fig. 8).

Figures 9a–d and 10a–d are similar to Fig. 8a–d except they represent data from later times. The

θ_e in the HRSKF3.3KM simulation runs, however, compare favorably with the observed values, especially up to the middle troposphere as can be seen from Figs. 9b, d, 10b and d. Figure 10 also shows the effect of the improved initial analysis on the simulation has decreased after about 48 h.

Figures 11 and 13a–c summarize the temperature and wind values for the BOBMEX buoy (13° N, 87° E) and the four model runs. The error in temperature for the HRSKF3.3KM runs is of the same order as the FDDA run; the temperature error for the HRSGR3.3 run was lower by 0.4–0.5 K. Nielson-Gammon (2004) provides evi-
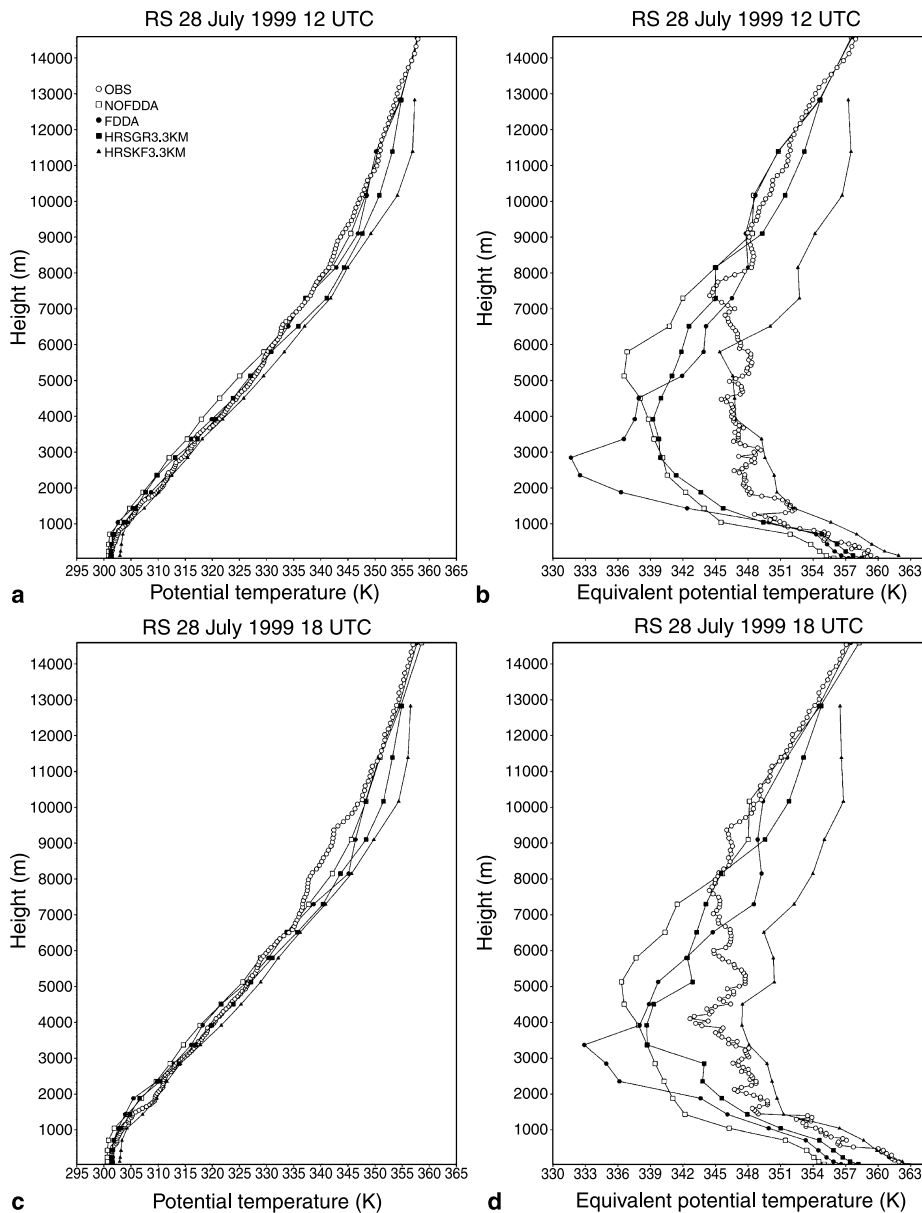
Fig. 10a–d. Same as Fig. 8a–d, except for 28 July 1999 12 and 18 UTC
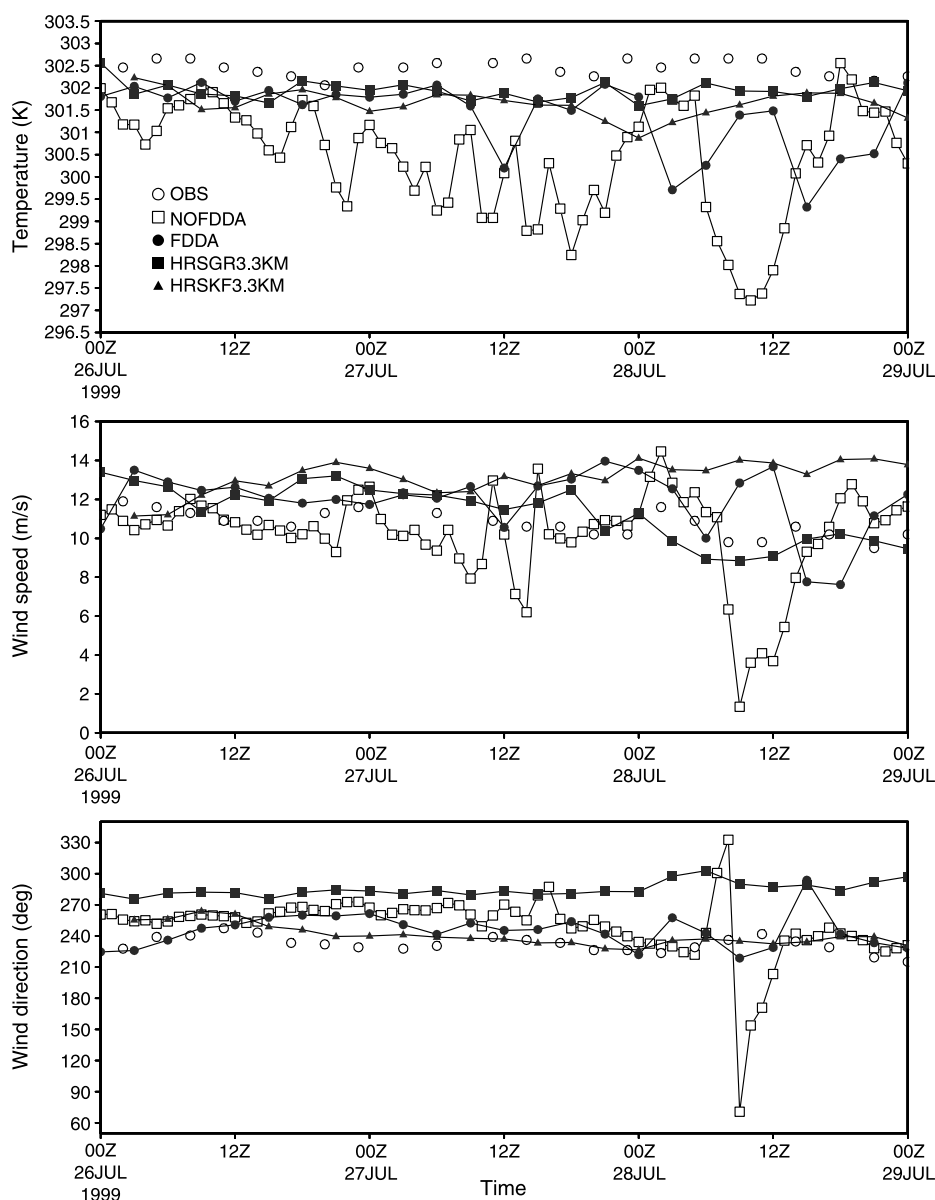
Fig. 11. Comparison of model results with BOBMEX buoy observations

dence of a root mean square (rms) error of wind speed between $1.3\,\mathrm{m\,s^{-1}}$ and $2.5\,\mathrm{m\,s^{-1}}$ when nudging was adopted, which is lower by two to three times as compared to results without nudging. The FDDA run yielded an rms error of wind speed of $1.37\,\mathrm{m\,s^{-1}}$ for the buoy observations. The error is $0.62\,\mathrm{m\,s^{-1}}$ for the HRSGR3.3KM and $2.98\,\mathrm{m\,s^{-1}}$ for HRSKF3.3KM. The rms errors of wind speed for the buoy observations in the NOFDDA run were higher by 1.5/3.5 times as compared to the FDDA/HSRGR3.3KM runs. Due to nudging, the absolute error was reduced by 188% for temperature, 43% for wind speed, and 72% for wind direction for the buoy observations. Compared to the FDDA run, the abso-

lute error for HRSGR was lower for temperature by $0.37\,\mathrm{K}$ and for wind speed by $0.62\,\mathrm{m\,s^{-1}}$. However, compared to the FDDA run, the absolute error for the HRSGR3.3KM run for wind direction was higher by $50°$.

The results of the HRSKF3.3KM indicate that except for wind direction and temperature error, which were comparable with the FDDA run, the error in the wind speed was even higher than the NOFDDA run. Cox et al. (1998) have proposed a desired forecast accuracy of $30°$ for wind direction, $2.5\,\mathrm{m\,s^{-1}}$ for wind speeds greater than $10\,\mathrm{m\,s^{-1}}$, $1\,\mathrm{m\,s^{-1}}$ for other wind speeds, $2\,\mathrm{K}$ for temperature, $2\,\mathrm{K}$ for dew point depression and $1.7\,\mathrm{hPa}$ for SLP. The model wind direction for
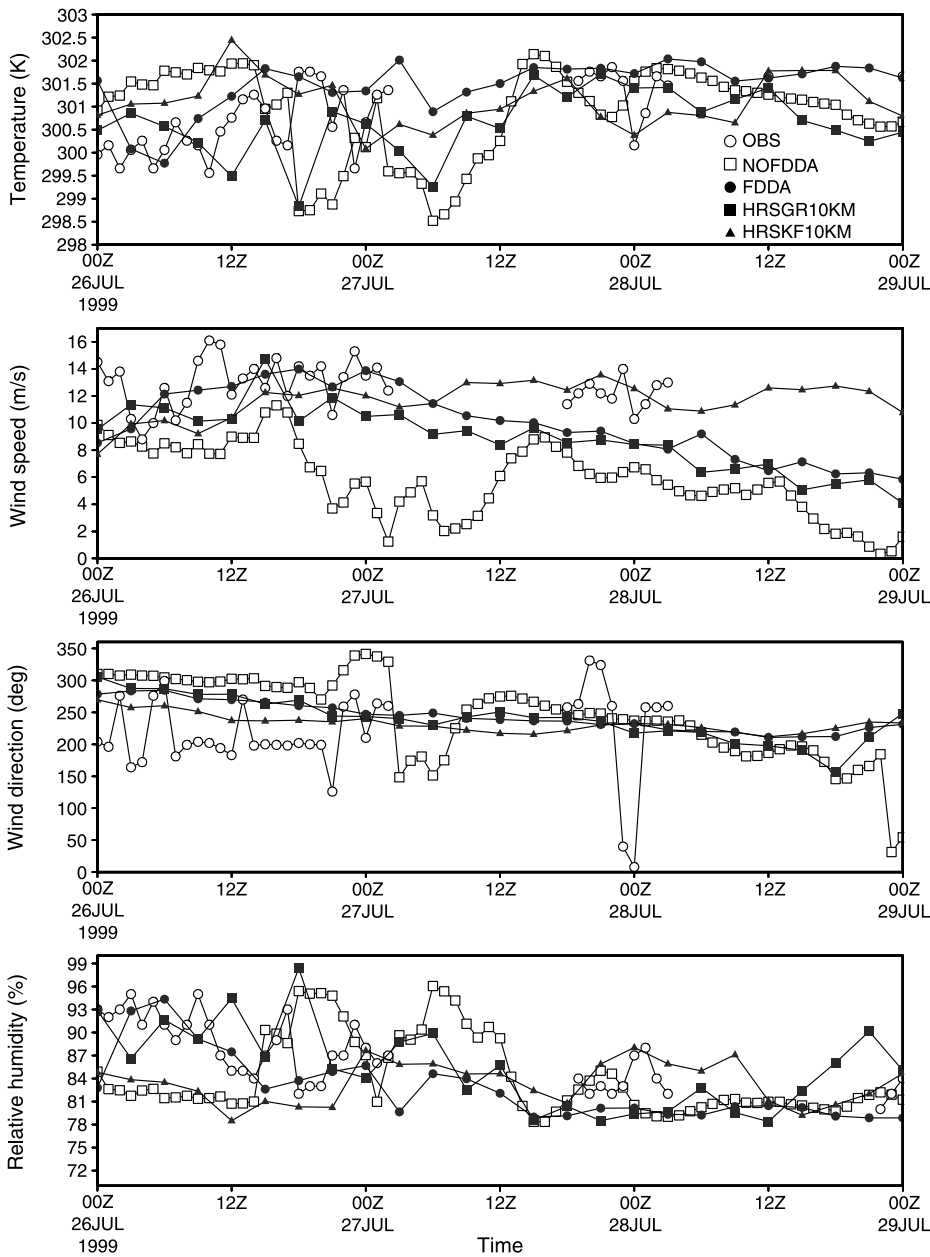
Fig. 12. Comparison of model results with BOBMEX ship observations

the FDDA simulation has a less westerly bias of $-15.3°$, the HRSKF3.3KM run shows a bias of $-14.3°$ and the NOFDDA simulation shows a bias of $-19.5°$. The results of the high-resolution HRSGR run show lower errors for temperature and wind speed, while the HRSKF run shows lower errors for wind direction as compared to the FDDA run. The fact that at least one of the high-resolution runs have higher errors than the FDDA run is partly because the traditional verification schemes have been used and also that the FDDA run has assimilated observations using the nudging approach. Despite the lower vertical

levels and smaller grid size, the FDDA simulations of temperature, wind speed and wind direction compare favorably with buoy observations.

During BOBMEX-99, data from a sonic anemometer and fast response humidity sensor was also available on board the ORV Sagar Kanya (Bhat and Ameenulla 2000). These data (10 Hz sample averaged over 360s, at 11.5 above surface) form part of the slow data and are compared here with the MM5 model results. Figures 12 and 13d–g summarize the temperature, wind and humidity from the BOBMEX ship and the four model runs. Since the 3.3 km do-
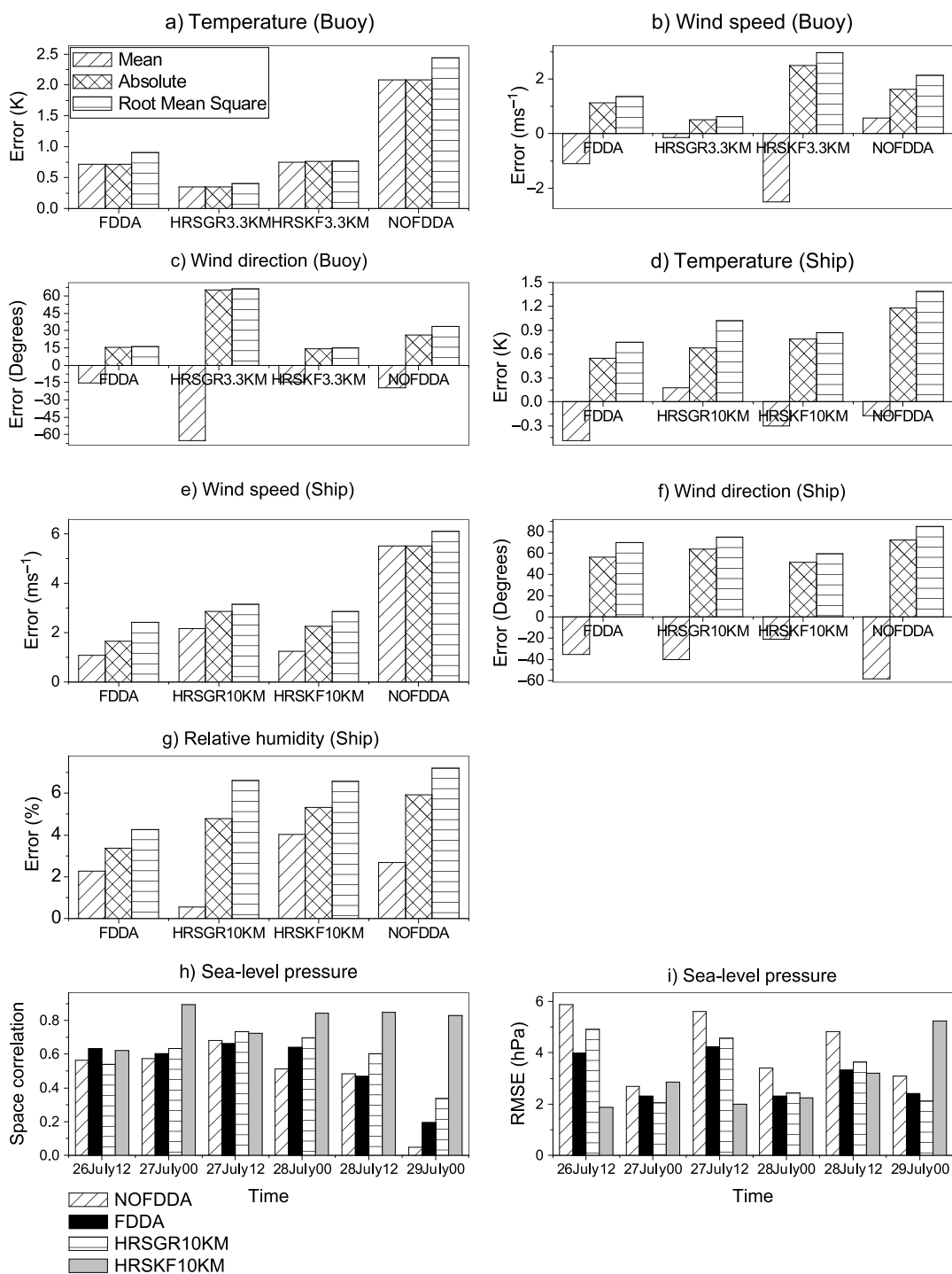
Fig. 13a–c. Mean error, absolute error and the root mean square (rms) error of difference for temperature, wind speed, and wind direction between the BOBMEX buoy observations and the MM5 model simulations for 26–29 July. (**d–g**) Mean error, absolute error, and the rms error of difference for temperature, wind speed, wind direction, and relative humidity between the BOBMEX ship observations and the MM5 model simulations for 26–29 July. (**h, i**) Space correlation and rms error of the SLP field for MM5 simulations with respect to NCEP reanalysis for a region 10° × 10° around the depression center for the July 1999 case

main did not contain the ship location throughout the entire duration, the comparison of the NOFDDA and FDDA runs are performed with

the 10 km domains. The statistical measures for wind direction are calculated for those times where the differences between the model predic-

tions and the observations are within $180°$ (Buckley et al. 2004). The FDDA run yielded a rms wind speed error of $2.42 \, \text{m s}^{-1}$ and was lower by 2.5 times than the NOFDDA run. As obtained by Nielson Gammon (2004), the above finding is similar to the rms error of wind speed of $1.3 \, \text{m s}^{-1}$ and $2.5 \, \text{m s}^{-1}$ when nudging was employed. The errors for wind speed in the HRSGR10KM and HRSKF10KM runs were higher by $0.5 \, \text{m s}^{-1}$ as compared to the FDDA run. Also, for the ship observations, the absolute error was reduced due to nudging by 114% for temperature, 234% for wind speed, 30% for wind direction and 76% for relative humidity.

Figure 13d–g clearly shows that the high-resolution runs have large absolute errors for all the variables as compared to the FDDA run. This result is due to the traditional verification measures and the absence of assimilation in the high-resolution runs. All the above results indicate that the quantitative improvement seen in the meteorological variables due to nudging is consistent with the results of the earlier impact studies due to nudging.

3.1.4 The July 1999 depression simulations' space correlation and rms error of SLP

To further quantitatively assess the impact of the improved analysis, a box with a $10° \times 10°$ domain was identified over the center of the depression, which was the location of the minimum NCEP reanalysis SLP. Figure 13h, i show the space correlation and rms errors of the SLP field for the four model runs over the $10°$ box. The $10° \times 10°$ domain box chosen in Fig. 13h, i did not completely fit within the 3.3 km domain, so the high-resolution run comparison was performed with the 10 km domains.

The space correlation of the SLP field in the FDDA simulation is higher (0.13) compared to the NOFDDA simulations until 27 July 1999 00 UTC; after this date, the space correlation is comparable to the NOFDDA simulation. Furthermore, the rms errors of the SLP field in the FDDA simulation are consistently lower by 2.0 hPa than the NOFDDA runs. This result suggests a positive and quantitative impact of the improved analysis resulting from the inclusion and assimilation of satellite and other conventional upper air and surface meteorological data

in the model. A comparison of the space correlation and the rms errors of SLP for the FDDA run as compared to the HRSGR10KM and HRSKF10KM runs show that the high-resolution runs have more accurate spatial correlations and a lower rms error with HRSKF, which shows a better performance than the HRSGR.

The improvement in the skill of the high-resolution runs seen in Fig. 13h–i is due to the fact that the verification is over a box of $10° \times 10°$ and not over a point observation. The statistical significance of the differences between the FDDA and the NOFDDA results in Fig. 13a–i have been calculated using the two-tailed student's t statistics and were found to be statistically significant at a level of 95%.

3.1.5 Student's t-test for the MM5 July 1999 depression simulations

Student's t-tests were performed to determine whether the differences in the results between the NOFDDA and FDDA, as well as the high-resolution run (HRSGR10KM and HRSKF10KM), are statistically significant, Results were analyzed for the model runs over the entire model domain using 6 hourly SLP fields with respect to NCEP reanalysis and 3 hourly precipitation fields with respect to TRMM. Statistical significance tests at the 95% confidence level were performed for the differences between NOFDDA and FDDA with respect to the NCEP reanalysis (Fig. 14a). Similar significance tests of SLP were conducted with respect NCEP reanalysis but for differences between (i) HRSGR10KM and FDDA (Fig. 14c); (ii) HRSKF10KM and FDDA (Fig. 14e) and (iii) NOFDDA and HRSGR10KM (Fig. 14g).

Figure 14b, d, f and h are similar to Fig. 14a, c, and g except that Fig. 14b, d, f, and h refer to the 3 hourly precipitation amounts with respect to the TRMM observations. The shaded regions, in Fig. 14a–h are statistically significant at 95% level. Figure 14a and b show shaded patches (although less shaded in Fig. 14b), especially over the depression region indicating that the statistically significant differences exist at the 95% level between the NOFDDA and the FDDA runs. Figure 14c and e show the more significant patches for SLP are adjacent to the depression center, while for the precipitation (Fig. 14d, f), the shaded (significance) region is observed south

SLP (NOFDDA+FDDA, JULY 1999)

Rain (NOFDDA+FDDA, JULY 1999)

a

b

SLP (HRSGR10KM+FDDA, JULY 1999)

Rain (HRSGR10KM+FDDA, JULY 1999)

c

d

SLP (HRSKF10KM+FDDA, JULY 1999)

Rain (HRSKF10KM+FDDA, JULY 1999)

e

f

SLP (NOFDDA+HRSGR10KM, JULY 1999)

Rain (NOFDDA+HRSGR10KM, JULY 1999)

g

h
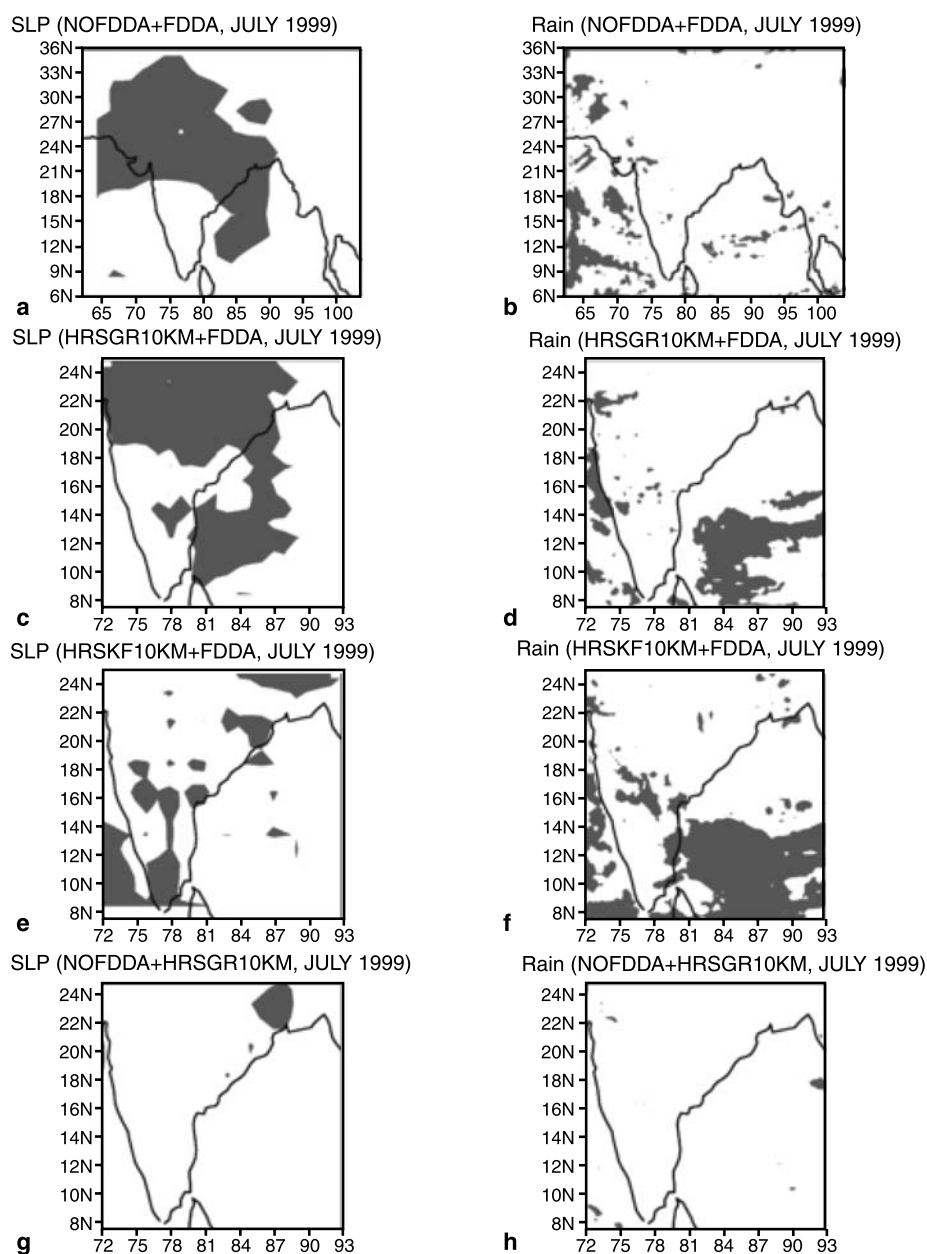
Fig. 14a–h. The statistical significance among the model experiments (NOFDDA, FDDA, HRSGR10KM, HRSKF10KM) of SLP and precipitation at 95% confidence level using Student's *t*-test. (**a**) and (**b**) refer to NOFDDA vs. FDDA for SLP and precipitation respectively. (**c**) and (**d**) refer to HRSGR10KM vs. FDDA for SLP and precipitation. (**e**) and (**f**) refer to HRSKF10KM vs. FDDA for SLP and precipitation. (**g**) and (**h**) refer to NOFDDA vs. HRSGR10KM. Areas statistically significant at 95% are shaded

of the depression and also on the west coast of India. Furthermore, Fig. 14g and h clearly highlight that the differences between the NOFDDA and the HRSGR10KM runs are not as statistically significant as compared to the differences with the FDDA.

3.2 Monsoon depressions during August and October 2003

3.2.1 Model evaluations of the NOFDDA and FDDA simulations

This subsection evaluates the impact of the combined assimilation of the MODIS temperature and humidity vertical profiles, QuikSCAT ocean surface wind vector, and the IMD upper-air and surface observations on the structure and spatial distribution of precipitation for August and October 2003 monsoon depressions. The model domain for both depression cases is shown in Fig. 2f and has a system of two nested domains with a horizontal grid spacing of 90 km (D1) and 30 km (D2). All the model results discussed for the depression cases correspond to the 30 km domain.

Figure 15a–l depict the SLP as well as the lower tropospheric wind and 24 h accumulated rainfall pattern for 27 August 2003 00 UTC
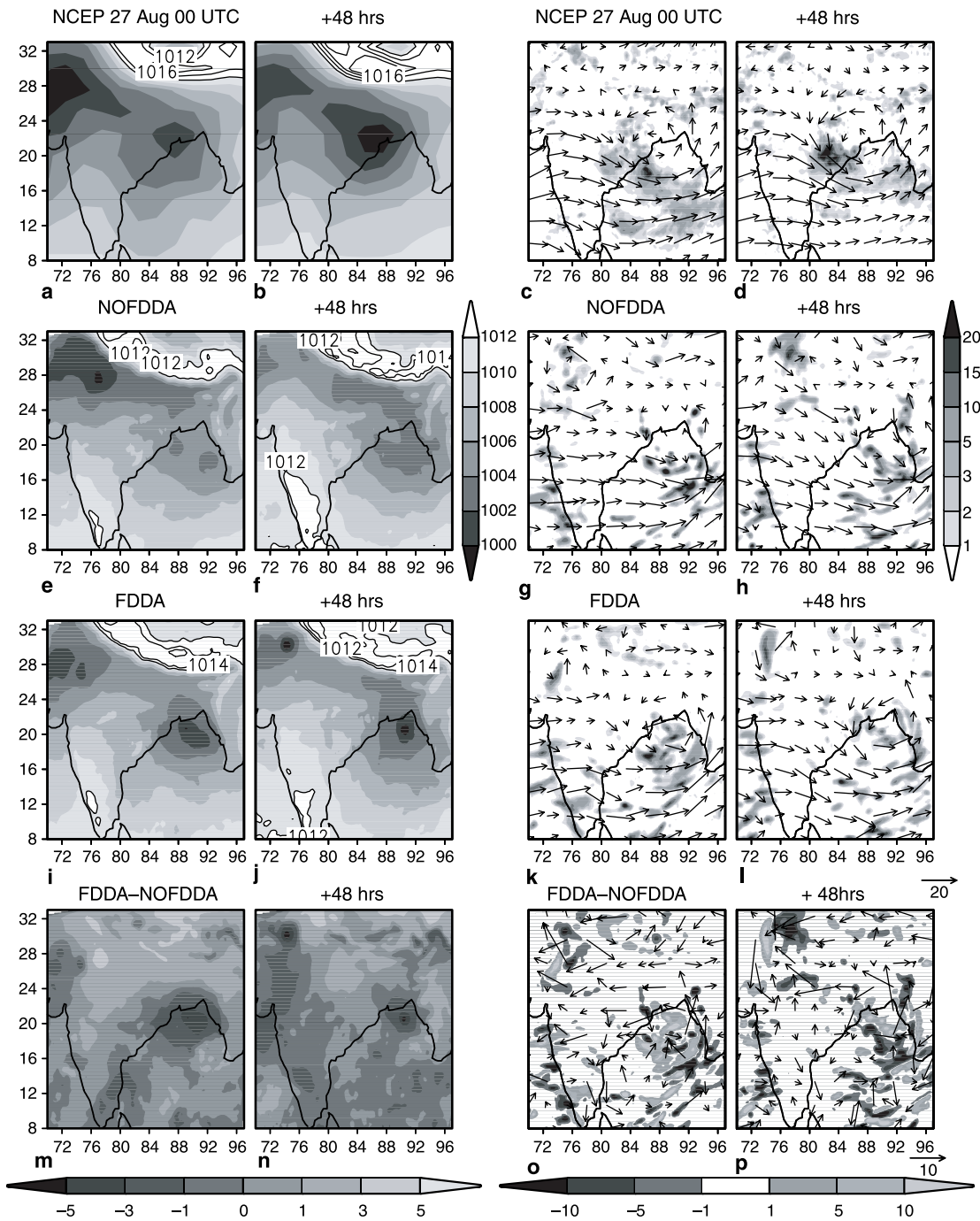
Fig. 15a–b. Sea-level pressure (hPa) for 27 August 2003 00 UTC and for 48 h of forecast of NCEP reanalysis, (**e–f**) NOFDDA and (**i–j**) FDDA. (**m–n**) Sea-level pressure difference (hPa) of NOFDDA from FDDA for the 27 August 2003 00 UTC and for 48 h of forecast. (**c–d**) Lower tropospheric winds (m s^{-1}) (850 hPa for NCEP reanalysis and $\sigma = 0.825$ for MM5 simulations) for 27 August 2003 00 UTC and for 48 h of forecast. Also shown are the 24 h accumulated TRMM rainfall (cm) and the model precipitation (cm) at 24 and 48 h of forecast, (**g–h**) NOFDDA and (**k–l**) FDDA. (**o–p**) Lower tropospheric wind difference (m s^{-1}) of NOFDDA from FDDA for 27 August 2003 00 UTC and for 48 h of forecast. Also shown the 24 h accumulated precipitation difference (cm) of NOFDDA from FDDA at 24 and 48 h of forecast

and 48 h of forecast time. Figure 16a–l are similar to Fig. 15a–l, except that 16a–l refer to 06 October 2003 00UTC and 48 h of forecast time,

respectively. MODIS provides vertical temperature and humidity profiles with high horizontal resolution (5 km) as compared with the coarser
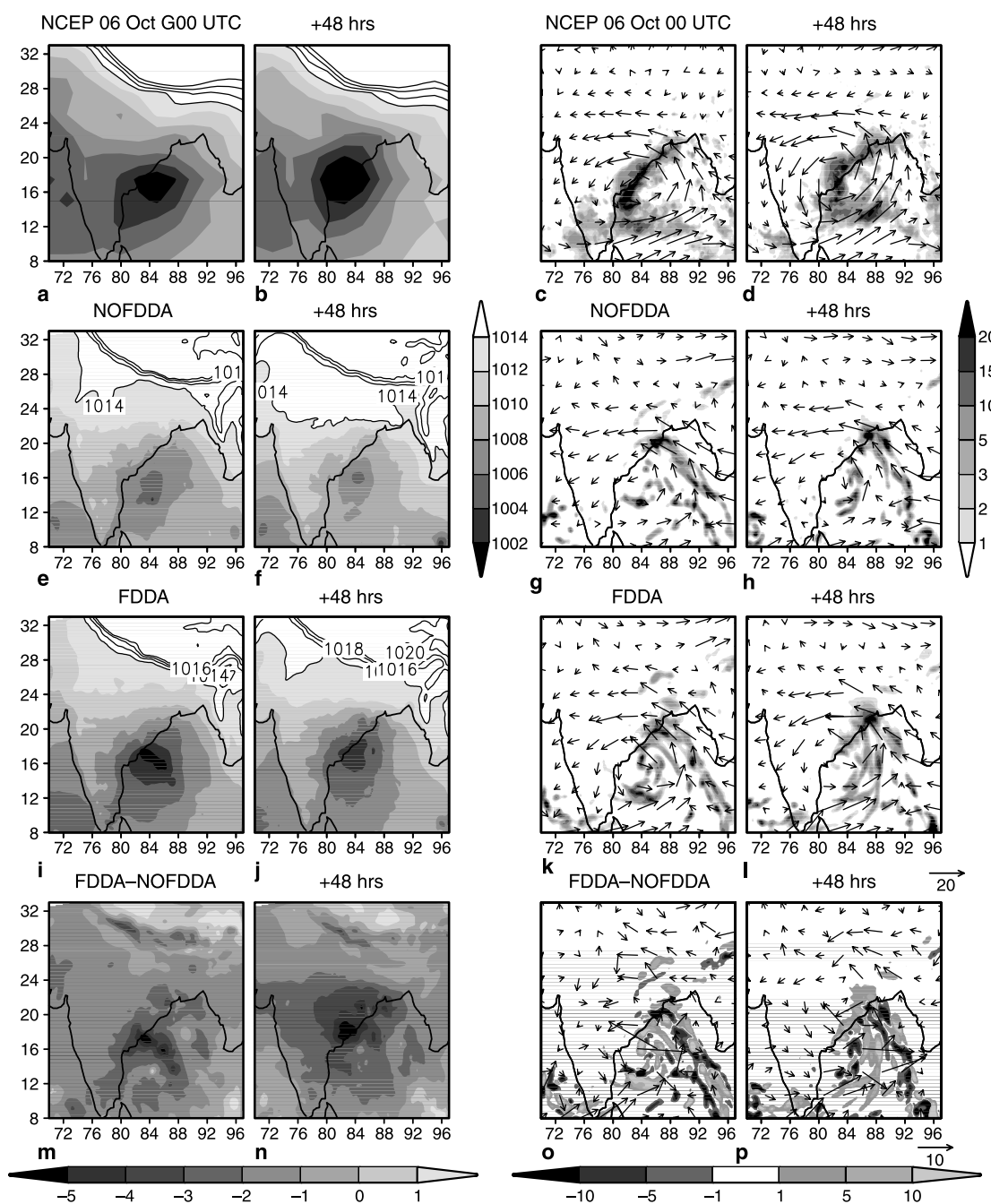
Fig. 16a–p. Same as Fig. 15a–p except for the October 2003 depression

horizontal resolution of NOAA-TOVS. The MODIS sensor, similar to the NOAA-TOVS, measures radiances in the infrared part of the spectrum and cannot provide information of the vertical profiles of temperature and humidity over the regions covered by thick clouds. Also, the MODIS sensor (similar to the NOAA-TOVS) is mounted on a polar orbiting satellite, and hence the number of passes over a region is also limited. Despite these limitations, the MODIS data still have utility in providing high-resolution horizontal measurements over cloud-free regions.

The improvements in the simulated horizontal structure of the SLP field from the two depression cases indicate the positive impact of the ingestion and assimilation of the MODIS, QuikSCAT and IMD data using analysis nudging. In both of the depression cases, the NOFDDA run fails to simulate the depression until 48 h (not shown). However, the FDDA run succeeded

in simulating the intensification of the system to the depression stage consistent with observations and the analysis (Figs. 15i and 16i). Also, both the depressions' central SLP in the NOFDDA simulation is higher by 4 hPa as compared to the NCEP reanalysis and to the FDDA simulations. Observations had indicated that the two depressions moved in a west-northwesterly direction and crossed land in the early morning hours of 28 August 2003 and 7 October 2003, respectively. The FDDA run reveals a delayed occurrence of landfall.

Figure 15m–p show the differences between the FDDA and NOFDDA results for the August depression, while Fig. 16m–p show the differences for the October depression. In the FDDA simulation for both the depressions, the negative values of SLP difference (3–5 hPa) in the immediate vicinity of the depression center at these times indicate a substantial improvement in the intensity simulation of the system.

The FDDA run (Figs. 15k, l and 16k, l) reproduced the intensification of the cyclonic circulation and the accompanying increase in the wind speed consistent with the transition from a low-pressure system to a depression, at and after 24 h of forecast. This was consistent with the observations including the NCEP reanalysis. The NOFDDA run simulated a weaker cyclonic circulation. The improved simulation of stronger cyclonic circulation in the FDDA run is possibly due to the assimilation of high-resolution QuikSCAT wind observations using analysis nudging.

For the August (October) depression case, the maximum TRMM rainfall at the end of 24 h of forecast was centered at 18° N 86° E (18° N, 83° E). With the subsequent movement of the depression in a west-northwesterly direction, the maximum TRMM rainfall was centered over the land at 19° N 82° E (18.5° N 83° E for the October case) after 48 h of forecast. Neither of the MM5 runs simulated the landfall and the maxima of rainfall over land at the end of 48 h of forecast for the August case. The FDDA run did simulate a relatively better large-scale structure of the spatial precipitation pattern at the end of 24 h of forecast time (Figs. 15k and 16k) as compared to the NOFDDA (Figs. 15g and 16g) run. However, differences exist between the TRMM data and the actual location, extent, and amount of rainfall in the FDDA run.

Similar to the above results, Das et al. (2003) also found that although nudging enhanced the rainfall amounts and also was responsible for eliminating spurious rainfall, difficulties occurred in simulating the exact location of rainfall maxima.

Unlike the BOBMEX and the August 2003 depression cases, the FDDA run from the October depression case reproduced the large-scale structure of the observed spatial precipitation pattern both at the end of 24 and at 48 h of forecast. In the vicinity of the depression, a cyclonic circulation appears in the difference field (Figs. 15o, 16o), indicating that the FDDA run simulated well the intensity of the depression. The maximum positive differences (Figs. 15o, p and 16o, p) in the precipitation field occur over the oceans and are 50–100 mm less as compared to the 1999 depression case.

For the August and October depression cases also, an exercise similar to the 1999 BOBMEX case was performed at various times on a 15° × 15° box centered on the depression center. The spatial correlation and the rms error of the SLP field in both the NOFDDA and FDDA runs with respect to the NCEP reanalysis were calculated (Fig. 17a–d). Overall, Fig. 17a, b indicate that the spatial correlation and rms error of the SLP field for the August depression are both higher (0.05 hPa) and lower (0.23 hPa), respectively for the FDDA run as compared to the NOFDDA run. This behavior is however, not uniformly observed at all times. The statistical significance of the differences between the FDDA and the NOFDDA results in Fig. 17a, b was found to be insignificant.

For the October case, a consistent increase (0.2 hPa) in the spatial correlation and a decrease (3.34 hPa) of the rms error of the SLP field for the FDDA run was obtained (Fig. 17c–d). The differences between the FDDA and the NOFDDA results were found to be statistically significant at the 95% level.

Figure 17a–d shows that the spatial correlation values of the SLP field for the August as well as the October depressions are uniformly higher (and thus have lower differences between the runs) than those of the BOBMEX depression case. It is to be noted that the BOBMEX depression was quite intense with the lowest SLP having values on the order of 994 hPa or higher,
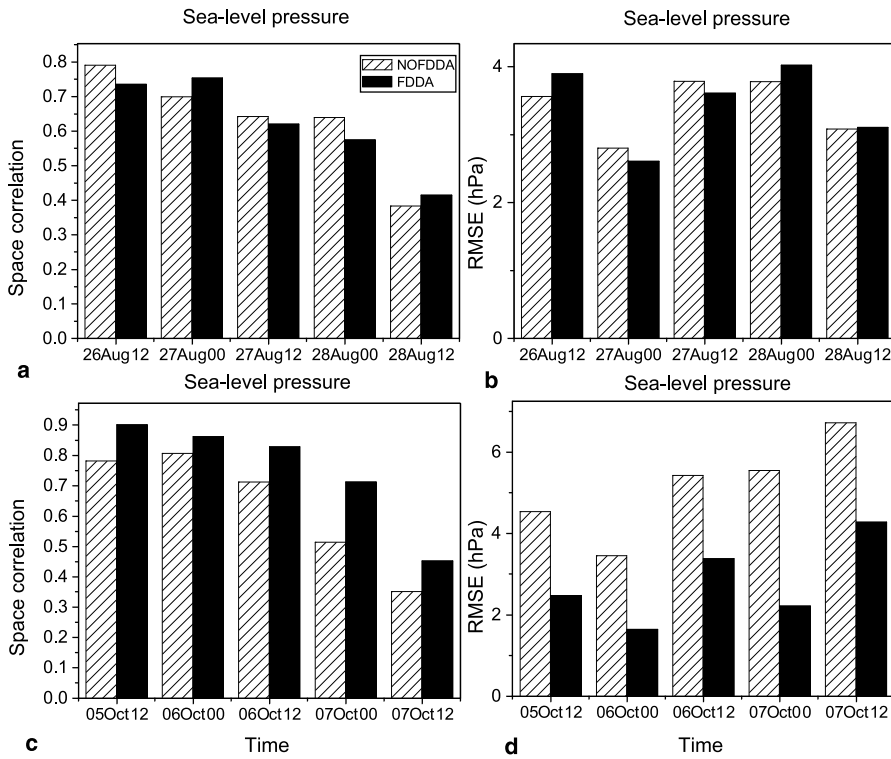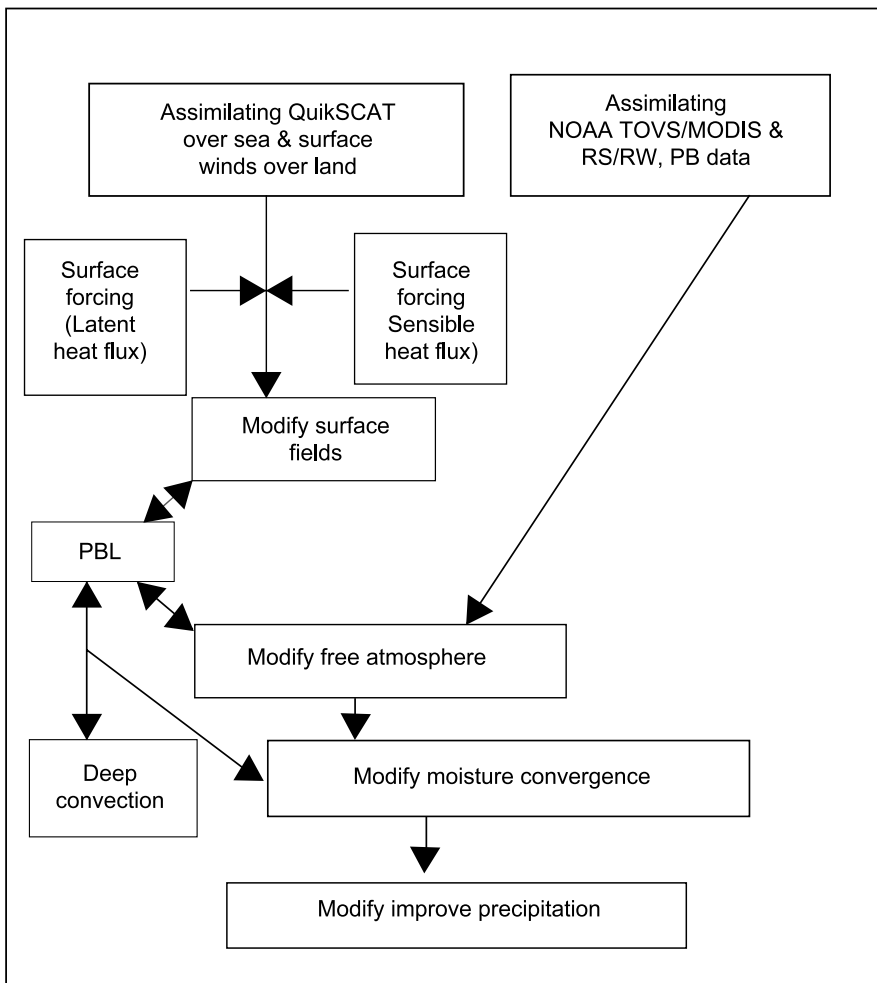
Fig. 17a–d. Spatial correlation and root mean square (rms) error of the sea-level pressure field for MM5 simulations with respect to NCEP reanalysis for a region $15° \times 15°$ around the depression center for the August and October 2003 case. (**e**) Schematic diagram of the likely feedbacks and processes that have contributed to improved prediction

while the lowest SLP for the August and October 2003 depression was on the order of 1000 hPa or higher. The larger differences seen in Fig. 13h and i for the BOBMEX case might be attributable to the inability of the model, without assimilation, to simulate and predict a very intense monsoon depression. Unlike the 1999 BOBMEX depression case, the rms error of the SLP field for the FDDA run (Fig. 17b) from the August depression case is marginally higher than the NOFDDA run at and after 48 h of forecast. However, the October 2003 depression clearly shows a smaller rms error in the FDDA run (Fig. 17d). Of the three depressions investigated in this study, the October 2003 case appears to have the largest impact due to the assimilation of satellite and IMD observations with respect to the spatial correlations and rms error of the SLP field.

4. Conclusions

The purpose of this study was to investigate the impact of data ingestion and assimilation of NOAA-TOVS/MODIS, QuikSCAT, RS/RW, pilot balloon sounding and surface measurements using analysis nudging on the prediction of three monsoon depressions over the Bay of Bengal. The resulting improvements in the simulation due to data assimilation are also compared with impact of increased model resolution (finer grid spacing) and the cumulus parameterization schemes.

Study results demonstrated the favorable impact of analysis nudging on the structure and associated precipitation pattern of the monsoon depressions. Compared to the HRSKF run, the FDDA run better simulated the 1999 depression in terms of SLP, cyclonic circulation and associated precipitation patterns. The HRSGR runs correctly simulated the movement and subsequent landfall of the depression. However, the HRSGR simulation failed to reproduce the weakening of the depression due to the frictional effects of overland movement. The FDDA run, on the other hand, simulated well the weakening of the 1999 depression after landfall. The simulation of the SLP by the Kain-Fritsch run is not as good as the Grell run. The results of this study indicate that, in terms of SLP, cyclonic circulation and the associated precipitation patterns the improve-

ments in the model performance due to data assimilation through analysis nudging are of a similar or equal magnitude to the improvements in model performance made by increased model resolution and the appropriate choice of cumulus parameterization.

Figure 17e shows the likely feedbacks and processes that could have resulted in the improved structure and spatial distribution of model precipitation due to the ingestion and assimilation of both satellite and conventional meteorological observations. The assimilation of the off-shore QuikSCAT surface wind vector and over-land surface winds, in addition to improving the representation of the surface winds, can create secondary forcing that modifies the simulation of surface fields. The improved surface fields can then influence the PBL and possibly the free atmosphere through improved vertical mixing processes. The assimilation of temperature and moisture profiles over the sea and land by employing NOAA-TOVS/MODIS data and over the land by employing radiosonde data, in addition to improvements in the thermodynamic structure, can also influence the moisture convergence and associated spatial distribution of precipitation patterns through the dynamic interaction of deep convection with the boundary layer.

The predicted SLP of the FDDA simulation for all three depressions considered here reproduced the large-scale structure of the depression, while the NOFDDA run simulated a much weaker system. The FDDA run for all three depressions also simulated an improved, better-developed and stronger cyclonic circulation as well as an improved, and relatively larger-scaled spatial distribution of precipitation compared with the NOFDDA simulations (except for the August 2003 depression). The results of this study indicate increased space correlation and reduced rms error of the SLP field for the FDDA run for all three depressions as compared to the NOFDDA run. The high-resolution model simulations resulted in higher spatial correlation and reduced rms error of SLP than that of the FDDA run.

The mean error, mean absolute error, and the rms error for the 1999 depression showed lower values for the FDDA run when compared with BOBMEX observations. Overall, the results of this study suggest that the assimilation

of both satellite and conventional meteorological data using analysis nudging had a favorable impact on the structure and spatial precipitation pattern of the monsoon depression for all three depressions. Furthermore, the differences between the FDDA and the NOFDDA results are statistically significant. Also, the results of this study strongly indicate that the quantitative improvement seen in the meteorological variables due to nudging is consistent with the results of earlier impact studies. The improvements in the FDDA run were uniformly better as compared to the NOFDDA runs for all three cases of depression.

Acknowledgements

References

Alapaty K, Niyogi D, Alapaty M (2001) An inverse technique for assimilating/adjusting soil moisture in the MM5. The 11th Penn State/NCAR MM5 User's Workshop, NCAR, Boulder, CO

Bhat GS, Ameenulla S (2000) Surface meteorological instrumentation for BOBMEX. P Indian A S-Earth 109: 221–8

Buckley RL, Weber AH, Weber JH (2004) Statistical comparison of regional atmospheric modeling system forecasts with observations. Meteorol Appl 11: 67–82

Cox R, Bauer BL, Smith T (1998) A mesoscale model intercomparison. Bull Amer Meteor Soc 79: 265–83

Das S, Dudhia J, Barker DM, Moncrieff M (2003) Simulation of a heavy rainfall episode over the west coast of India using analysis nudging in MM5. 13th PSU/NCAR Mesoscale Model Users Workshop, NCAR, Boulder, CO

Das Gupta M, Basu S, Paliwal RK, Mohanty UC, Sam NV (2003) Assimilation of special observations taken during the INDOEX and its impact on the global analysis-forecast system. Atmosfera 16: 103–18

Doyle JD, Warner TT (1988) Verification of mesoscale objective analysis of VAS and rawinsonde data using the March 1982 AVE/VAS Special Network Data. Mon Wea Rev 116: 358–67

Gal-Chen T, Schmidt BD, Uccellini LW (1986) Simulation experiments for testing the assimilation of geostationary satellite temperature retrievals into a numerical prediction model. Mon Wea Rev 114: 1213–30

Grell GA, Dudhia J, Stauffer DR (1994) A description of the fifth generation Penn State/NCAR mesoscale model (MM5). NCAR Technical Note TN-398 + STR National Center for Atmospheric Research, Boulder, CO

Kuo YH, Guo YR (1989) Dynamic initialization using observations from a hypothetical network of profiles. Mon Wea Rev 117: 1975–98

Lipton AE, Vonder Haar TH (1990) Mesoscale analysis by numerical modeling coupled with sounding retrieval from satellites. Mon Wea Rev 118: 1308–29

Lipton AE, Modica GD, Heckman ST, Jackson AJ (1995) Satellite model coupled analysis of convective potential in Florida with VAS water vapor and surface temperature data. Mon Wea Rev 123: 3292–304

Mass CF, Ovens D, Westrick K, Colle BA (2002) Does increasing horizontal resolution produce more skillful forecasts? Bull Amer Met Soc 83: 407–30

Mukhopadhyay P, Sanjay J, Cotton WR, Singh SS (2004) Impact of surface meteorological observations on RAMS forecast of monsoon weather systems over the Indian region. Meteorol Atmos Phys 90: 77–108

Nageswara Rao G (2001) Occurrence of heavy rainfall around the confluence line in monsoon disturbances and its importance in causing floods. P Indian A S-Earth 110: 87–94

Nielson-Gammon J (2004) Performance evaluation of profiler nudging in the MM5 meteorological model. Report to the Texas Commission on Environmental Quality, 26 pp. http://216.239.59.104/search?q-cache:iKuJQdrn01AJ:www.met.tamu.edu/temp/profnudg2.pdf

Pielke RASR (2002) Mesoscale meteorological modeling. Elsevier Publications, Academic Press, 676 p

Potty KVJ, Mohanty UC, Raman S (2000) Numerical simulation of monsoon depression over India with a high resolution nested regional model. Meteor Appl 7: 45–60

Rajan D, Mitra AK, Rizvi SRH, Paliwal RK, Bohra AK, Bhatia VB (2001) Impact of satellite derived moisture in a global numerical weather prediction model. Atmosfera 14: 203–9

Rajan D, Simon B, Joshi PC, Bhatia VB, Mitra AK, Paliwal RK (2002) Impact of NOAA/TOVS derived moisture profile over the ocean on global data assimilation and medium range weather forecasting. Atmosfera 15: 223–36

Roy Bhowmik SK (2003) Prediction of monsoon rainfall with a nested grid mesoscale limited area model. P Indian A S-Earth 112: 499–519

Roy Bhowmik SK, Prasad K (2001) Some characteristics of limited area model precipitation forecast of Indian monsoon and evaluation of associated flow features. Meteorol Atmos Phys 76: 223–36

Ruggiero FH, Sashegyi KD, Lipton AE, Madala RV, Raman S (1999) Coupled assimilation of geostationary satellite sounder data into a mesoscale model using the Bratseth analysis approach. Mon Wea Rev 127: 802–20

Sandeep S, Chandrasekar A, Singh D (2006) The Impact of AMSU data for the prediction of a tropical cyclone over India using a mesoscale model. Int J Rem Sens 27: 4621–53

Sikka DR, Sanjeeva Rao P (2000) Bay of Bengal Monsoon Experiment (BOBMEX) – a component of the Indian Climate Research Programme (ICRP). P Indian A S-Earth 109: 207–9

Singh R, Pal PK (2003) Impact of QuikSCAT derived wind fields on a mesoscale non-hydrostatic model. Mausam 54: 183–8

Stauffer DR, Seaman NL (1990) Use of four-dimensional data assimilation in a limited-area mesoscale model. Part I: Experiments with synoptic-scale data. Mon Wea Rev 118: 1250–77

Vaidya SS, Mukhopadhyay P, Trivedi DK, Sanjay J, Singh SS (2003) Prediction of tropical systems over Indian region using a mesoscale model. Meteorol Atmos Phys 86: 63–72

Venkata Ratnam J, Cox EA (2006) Simulation of monsoon depression using MM5: sensitivity to cumulus parameterization schemes. Meteorol Atmos Phys 93: 53–8

Xavier VF, Chandrasekar A, Singh R, Simon B (2006) The impact of assimilation of MODIS data for the prediction of a tropical low pressure system over India using a mesoscale model. Int J Rem Sens 27: 4655–76

Zhang DL, Wang XX (2003) Dependence of hurricane intensity and structure on vertical resolution and time-size. Adv Atmos Sci 20: 711–25